

T-3247

**The Measurement and Application
of the Gamma Ray to Charged Particle Branching Ratios
for the $d + t$ and $d + d$ Fusion Reactions**

By

Francis J. Wilkinson III

ProQuest Number: 10782825

All rights reserved

INFORMATION TO ALL USERS

The quality of this reproduction is dependent upon the quality of the copy submitted.

In the unlikely event that the author did not send a complete manuscript and there are missing pages, these will be noted. Also, if material had to be removed, a note will indicate the deletion.



ProQuest 10782825

Published by ProQuest LLC (2018). Copyright of the Dissertation is held by the Author.

All rights reserved.

This work is protected against unauthorized copying under Title 17, United States Code
Microform Edition © ProQuest LLC.

ProQuest LLC.
789 East Eisenhower Parkway
P.O. Box 1346
Ann Arbor, MI 48106 – 1346

T-3247

A thesis submitted to the faculty and the Board of Trustees of the Colorado School of Mines in partial fulfillment of the requirements for the degree of Master of Science (Physics).

Golden, Colorado

Date 4/16/86

Signed: Francis J. Wilkinson III
Francis J. Wilkinson III

Approved: F. E. Cecil
Dr. F. E. Cecil
Thesis Advisor

Golden, Colorado

Date 4/16/86

Signed: F. D. Schowengerdt
Dr. F. D. Schowengerdt
Head, Physics Department

Abstract

The absolute gamma ray detection efficiency and energy resolution for a large NaI(Tl) gamma ray spectrometer were measured between 2.6 and 16.1 MeV. The efficiency of the NaI(Tl) detection system was found to be relatively constant between the energies of 2.6 and 16.1 MeV for the no coincidence (25%) and the anticoincidence (15%) detection modes, while the pair-coincidence mode varied from .5% to 5% over the same energy range. The energy resolution (fwhm) of the detection system for this same energy range varied from 13% and 6%.

The $\Gamma_{\gamma_0}/\Gamma_{\alpha}$ branching ratio for the $d + t$ and Γ_{γ}/Γ_p branching ratio for the $d + d$ reactions were measured and found to be roughly constant between deuteron bombarding energies of 45 and 150 keV. The $d + t$ measurements utilized pair-coincidence spectrometry in conjunction with the pulse-shape discrimination technique. The weighted average value of $\Gamma_{\gamma_0}/\Gamma_{\alpha} = (5.4 \pm 1.3) \times 10^{-5}$. The anticoincidence detection mode was used in the $d + d$ measurements. The weighted average value for $\Gamma_{\gamma}/\Gamma_p = (1.2 \pm 0.3) \times 10^{-7}$.

Table of Contents

	Page
Abstract.....	iii
List of Figures.....	vi
List of Tables.....	viii
Acknowledgements.....	ix
 Chapter I. Introduction.....	 1
 Chapter II. Characterization of the Detection System..	 7
Section One. The Design of the Detection System....	7
Section Two. The Evaluation of the Detection System	10
Part One. The Experimental Set-Up.....	10
Part Two. The Calculational Procedure.....	14
Part Three. The Experimental Results.....	17
 Chapter III. The Measurement of the $d + t$ Reaction	
at Low Energies.....	26
Section One. Introduction.....	26
Section Two. Experimental Procedure.....	29
Section Three. The Calculational Procedure.....	33
Section Four. Experimental Results and Discussion.	39
 Chapter IV. The Measurement of the $d + d$ Reaction	
at Low Energies.....	45
Section One. Introduction.....	45

Section Two. Experimental Procedure.....	48
Section Three. The Calculational Procedure.....	50
Section Four. Experimental Results and Discussion.	51
Chapter V. The Application of the $d + t$ and $d + d$ Gammas as Fusion Plasma Diagnostics.....	56
Section One. Gamma Reactivities.....	56
Section Two. Estimated Gamma Yields.....	58
References Cited.....	65
Appendix. Reaction Yields.....	68

List of Figures

	Page
1. Scattering chamber, detector assembly, and associated signal processing.....	9
2. Energy level diagram for the $^{11}\text{B} + p$ reaction....	12
3. Detector assembly, scattering chamber and charged particle accelerator.....	13
4. The no coincidence, anticoincidence, and pair-coincidence spectra for the $^{11}\text{B}(p,\gamma)$ reaction.....	18
5. Typical charged particle spectrum for the $^{11}\text{B}(p,\alpha)^8(2\alpha)$ reaction.....	20
6. The measured absolute gamma ray detection efficiencies as a function of energy.....	23
7. Detector energy resolution as a function energy.....	25
8. Energy level diagram for the $d + t$ reaction..	28
9. $d + t$ experimental set-up.....	30
10. Pair-coincidence and pulse-shape discrimination circuitry for the $d + t$ measurements.....	34
11. TAC spectrum for the $d + t$ reaction.....	35
12. $d + t$ gamma spectrum along with calibration spectra.....	40
13. Measured branching ratio for the $d + t$ reaction..	44

14. Energy level diagram for the $d + d$ reaction.....	47
15. $d + d$ gamma spectrum.....	52
16. Measured branching ratio for the $d + d$ reaction..	55
17. The $d + t$ and $d + d$ reactivities as a function of plasma temperatures.....	59
18. Detector placement outside the TFTR.....	62
19. Estimated gamma yields.....	63

List of Tables

	Page
1. Fusion gamma reactions.....	3
2. Detection efficiency data.....	21
3. $d + t$ experimental data.....	41
4. $d + d$ experimental data.....	54

Acknowledgements

In some regards this is the most difficult portion of my thesis to write, since there are so many people I would like to thank. I am grateful to my father and mother for all of the encouragement that they have given me. I am also thankful to my brothers: Michael, Thomas, Gerard, Patrick, and Christopher; and to my sister, Anne Marie; for each one of them has helped me become the person I am.

I would like to thank Professor Ed Cecil, my thesis advisor, for the patience and insight that he has shared with me. The efforts which we have spent together have lead to the rewarding results that I am proud to present in this thesis.

I appreciate the useful comments and suggestions that the remaining members of my thesis committee, Drs. Frank Schowengerdt, Bob McAllister, Guy Towle and Steve Daniel, made on the first version of this thesis.

Over the past five years I have made many friends in the classroom, in the laboratory and on the basketball court. I am grateful to these friends for the academic, social, and spiritual times we have spent together. These special people include: Dave Cole, Roger Dalke, Tim and Becky Deignan, Dave and Shar Fobare, Jim and Linda Madsen,

Jean Mathews-Powers, Rick Powell, John Scorby, Chris Walker, and Wendy Calvin.

I would like to thank two special members of the Department of Physics staff, they are: Ms. Faye West, the department secretary and one of the kindest people I've ever met; and Jack Kintner, the machine shop supervisor, who shared his talents while helping us construct the experimental apparatus.

I would also like to acknowledge the assistance of the Nuclear Physics Group at the University of Colorado. In particular Professors Bob Ristinen and Jim Shephard for several useful conversations.

The work that has been presented in this thesis has been supported by the U.S. Department of Energy under Contract No. DE AC02 83ER40091.

For all those that have helped me grow in academic insight and as a person, whether they are acknowledged here or not, they are all remembered in my thoughts and in my prayers.

...It seems that life is not easy for any of us. But what of that? We must have perseverance and above all confidence in ourselves. We must believe that we are gifted for something, and this thing, at whatever cost, must be attained. Perhaps everything will turn out very well, at the moment we least expect it...

Madame Curie, March 18, 1894

Chapter I. Introduction

The increasing demand for more plentiful sources of energy is not something new. The need to solve the problems associated with delivering reliable, safe, and economical power have been with us since the industrial revolution. Scientists and engineers have continually sought out and developed new methods to satisfy growing energy needs. Today we are faced with these same problems. But this does not give the complete picture.

Presently we are also faced with a nearly insatiable need for energy, thus the need for *renewable* energy sources. The U. S. Government through the Department of Energy (DOE) has funded the controlled thermonuclear fusion reaction (CTFR) program in an effort to address this problem.

The fusing of light nuclear particles together as a means to supply electrical energy is attractive for several reasons. Fusion energy is appealing for these primary reasons, briefly; the fusion reaction supplies an abundant amount of energy per reaction; the proposed fusion reactor fuels are quite plentiful, consequently making fusion power relatively economical once the initial investments are made; and finally the hazardous nuclear

waste associated with fusion reactors will be much less a problem than that accompanying the production of fuels and operation of fission reactors.

The difficulties that the scientific and engineering communities have encountered in an attempt to experimentally create conditions in which the proper fuel density, temperature, and confinement time lead to a net output of energy by a reactor, are numerous.

One of the problems that has been faced is the inability to satisfactorily measure fusion plasma temperatures during test runs. It is crucial to know the plasma temperature as accurately as possible since it indicates how near the fusion plasma is to breakeven for a given fuel density and confinement time.

The techniques which have been primarily used to determine plasma temperatures fall into two separate categories (Ma78 and Wh79). The ion temperature can be analyzed by neutron spectroscopy, Doppler broadening of impurity lines, and infrared laser scattering. Secondly the electron temperature can be found by measuring magnetic bremsstrahlung or synchrotron radiation, or by using the principle of Thomson scattering to measure the Doppler spread in frequency of light re-radiated by the electrons.

Since several of the exothermic fusion reactions emit

prompt monoenergetic gamma rays of high energy, it has been suggested that these gammas could be used to measure fusion plasma temperatures (Me79 and Me82). In fact the 5.5 MeV gamma rays from the $D(p,\gamma)^3\text{He}$ fusion reaction have been observed during the hydrogen neutral beam heating of a deuterium plasma in Doublet-III (Ne84).

A list of fusion gamma reactions is given in Table One along with the energy of the emitted gamma ray. The

Table One. Fusion gamma reactions.

<u>Reaction</u>	<u>Gamma ray energy (MeV)</u>
$P + D \rightarrow \gamma + {}^3\text{He}$	5.5
$P + T \rightarrow \gamma + {}^4\text{He}$	19.7
$D + D \rightarrow \gamma + {}^4\text{He}$	23.8
$D + T \rightarrow \gamma + {}^5\text{He}$	16.7
$D + {}^3\text{He} \rightarrow \gamma + {}^5\text{Li}$	16.4
$D + {}^4\text{He} \rightarrow \gamma + {}^6\text{Li}$	1.5
$T + T \rightarrow \gamma + {}^6\text{He}$	12.3
$T + {}^3\text{He} \rightarrow \gamma + {}^6\text{Li}$	15.8
$T + {}^4\text{He} \rightarrow \gamma + {}^7\text{Li}$	2.5
${}^3\text{He} + {}^3\text{He} \rightarrow \gamma + {}^6\text{Be}$	11.5
${}^4\text{He} + {}^3\text{He} \rightarrow \gamma + {}^7\text{Be}$	1.6
$P + {}^7\text{Li} \rightarrow \gamma + {}^8\text{Be}$	18.0 and 15.0
$P + {}^{11}\text{B} \rightarrow \gamma + {}^{12}\text{C}$	16.1, 11.7 and 4.4

listed fusion gamma rays which have energies above 10 MeV are good candidates for fusion temperature diagnostics since these gammas could easily be differentiated from the lower energy gammas that result from neutron activation.

The method by which the fusion gammas will indicate the plasma temperature is actually quite simple. The number of nuclear reactions is given by the nuclear reaction rate R ,

$$R = n_1 n_2 (1 + \delta_{12})^{-1} \langle \sigma v \rangle_{12}. \quad (I-1)$$

Here n_1 and n_2 are the number densities of the fusion plasma constituents and $\langle \sigma v \rangle$ is a reaction rate parameter known as the reactivity. The Kronecker delta is introduced to eliminate double counting when the constituents 1 and 2 are identical. The reactivity for a reaction can be related to the equilibrium plasma temperature through the velocity distribution of the interacting particles and the reaction cross section for the particles. The reactivity will be discussed in more detail in the concluding chapter of this thesis. It is clear then that if the reaction rate is known the plasma temperature can be determined directly.

The reaction rate or number of fusion events can be determined by measuring the gamma yield alone, since the cross sections for the charged particle branch and the

gamma ray branch of the nuclear reaction are related by the branching ratio. For the $d + t$ reaction the expression is written as:

$$\sigma_{T(d,\gamma)^5\text{He}} = (\Gamma_{\gamma_0} / \Gamma_{\alpha}) \sigma_{T(d,n)^4\text{He}}. \quad (\text{I-2})$$

The success that can be achieved in implementing the fusion gamma ray diagnostic technique depends on how accurately the gamma ray to charged particle branching ratio is known at fusion plasma energies.

The fusion reactions which are discussed in this thesis are the $d + t$ and $d + d$ reactions. Both of these reactions have dominant charged particle branches. The major portion of the work which is presented here involves the results of the measurement of the gamma ray to charged particle branching ratios for these two reactions.

Recently measurements of two of the other fusion gamma reactions, the $^3\text{He} + d$ (Ce85 and Co85) and $^{11}\text{B} + p$ (Sc85) reactions, have been carried out in this laboratory using similar experimental techniques.

The remaining discussion in this thesis is divided into four chapters. The experimental apparatus that was used to determine the branching ratios is discussed in Chapter II. Then in Chapters III and IV the measurements of the $d + t$ and $d + d$ fusion gammas are presented. The

gamma ray to charged particle branching ratios are also given. Finally in Chapter V the application of the $d + t$ and $d + d$ fusion gammas as a fusion plasma thermometer is given.

Chapter II. Characterization of the Detection System

The level of accuracy obtained in measuring the cross sections and branching ratios for the $d + t$ and $d + d$ reactions was largely determined by how well the detection system was designed. This chapter describes the design of the NaI(Tl) detection assembly and the associated signal processing. The results of the measured absolute detection efficiency and energy resolution of the gamma ray spectrometer are also presented in this chapter.

Section One. The Design of the Detection System

The primary design consideration was to insure that the detection system would be sensitive enough so that it would have the ability to detect the low level gamma count rates that were expected in the $T(d,\gamma)^5\text{He}$ and $D(d,\gamma)^4\text{He}$ reactions. This was accomplished by surrounding a 4" diameter by 4" long NaI(Tl) "plug" detector with a 12" diameter by 8" long NaI(Tl) longitudinally split annulus. The plug detector was mounted with a single 3 1/2 in. photomultiplier tube (PMT), while each optically isolated half of the annulus was mounted with three 3 1/2 in. PMT's. The through well of the annulus was lined with only .010" thick aluminum in order to minimize the

attenuation of gammas between the plug detector and the annulus.

The NaI(Tl) scintillator material was selected for the gamma ray spectrometer because of its good energy resolution and relatively good detection efficiency. The detector was manufactured by the Harshaw Chemical Company.

The detector and associated signal processing are shown schematically in Figure One. During measurements the plug detector was situated so that it would be flush with the front face of the annular detector as shown schematically in the figure. The system, as shown, could be used in four different detection modes. These modes were:

(1) *Summed spectrometry.* In this mode the signals from each of the three gain-matched detector elements were summed to approximate the effect of a 12" diameter by 8" long crystal.

(2) *Anticoincidence spectrometry.* The two half-annuli could also be operated in anticoincidence with the central detector for Compton suppression and cosmic ray suppression. The anticoincidence condition blocks the processing of signals from the central detector when a pulse greater than 600 keV is received from either half-annulus.

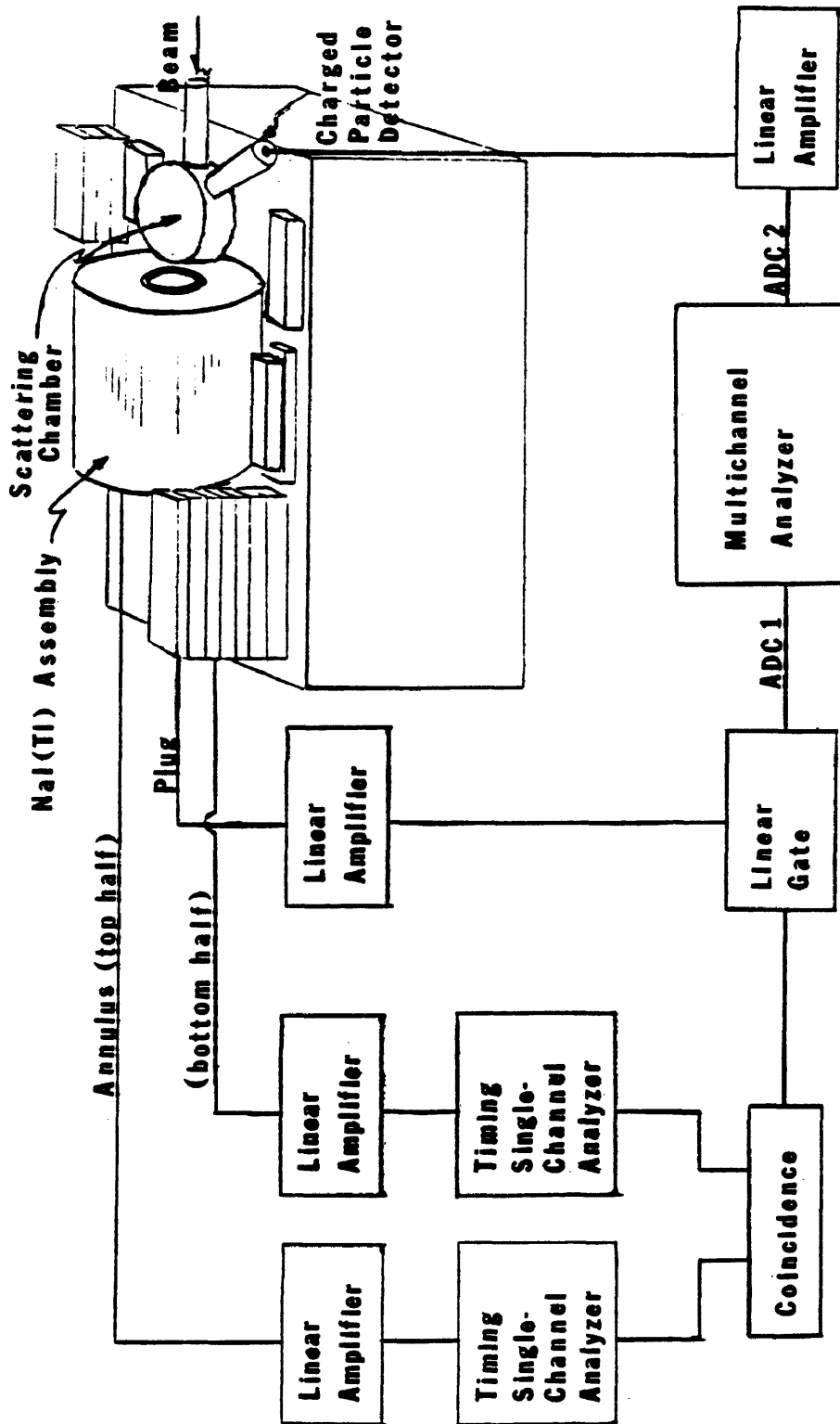


FIG. 1. Scattering chamber, detector assembly and associated signal processing.

(3) *No Coincidence Spectrometry.* In this mode only the ungated pulses from the plug detector are processed and displayed in the gamma spectrum.

(4) *Pair-coincidence spectrometry.* The simultaneous detection of a 511 keV annihilation gamma, actually any signal between the 300 and 600 keV window, in each half of the annulus, is required in order to open the gate which processes the signal from the central detector. In this manner the second escape peak of the gamma of interest is discerned at the expense of overall detection efficiency. This method is also effective in eliminating both Compton scattering and cosmic ray background.

The NaI(Tl) detector assembly was surrounded with lead shielding in order to aid in eliminating signals due to cosmic rays and natural gamma background. Paraffin shielding was added to help keep neutrons generated at the target from scattering back into the detector.

Section Two. The Evaluation of the Detection System

Part One. The Experimental Set-Up

The detection system was calibrated in energy and absolute detection efficiency by utilizing an intensity

calibrated gamma ray source, ^{228}Th with $E_\gamma=2.61$ MeV, and the resonant nuclear reaction $^{11}\text{B}(p,\gamma)^{12}\text{C}$ at $E_p=163$ keV. The decay scheme and energy level diagram for this charged particle reaction, as shown in Figure Two, indicates that the reaction yields gammas at energies of 4.44, 11.67, and 16.11 MeV. This is a result of the decay of the 16.11 MeV 2^+ excited state in ^{12}C to either the 4.44 MeV 2^+ excited state or the ^{12}C ground state.

The gamma rays from the $^{11}\text{B}(p,\gamma)^{12}\text{C}$ were produced by using the Cockcroft-Walton charged particle accelerator which is located in the Applied Nuclear Physics Laboratory of the Colorado School of Mines. The accelerator, which is capable of delivering a positively charged beam of light ions with energies of up to 170 KeV and beam currents of 20 μA , was used to generate the gammas by bombarding a thick target of natural metallic boron with 163 keV protons.

The experimental arrangement of the accelerator, target chamber, and detectors, as shown in Figure Three illustrates how the alpha particle spectrum from the $^{11}\text{B}(p,\alpha)^8\text{Be}$ branch of the $^{11}\text{B} + p$ reaction could be measured simultaneously with the $^{11}\text{B}(p,\gamma)^{12}\text{C}$ gamma spectrum.

The silicon surface-barrier charged particle detector

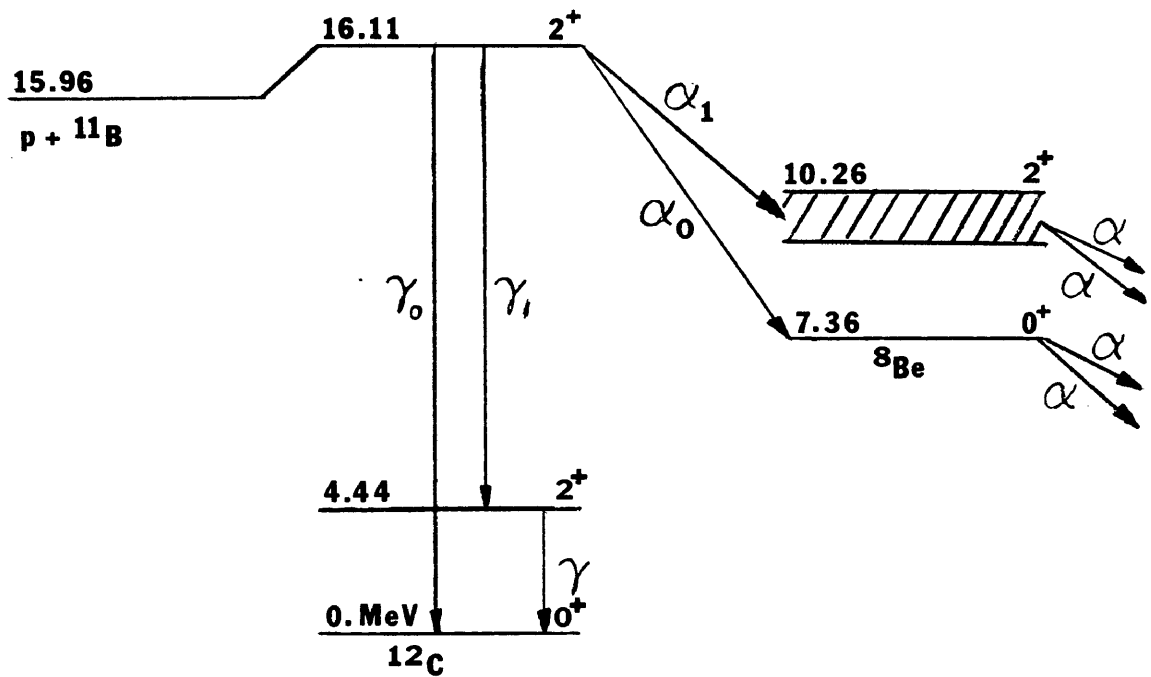


FIG. 2. The $^{11}\text{B} + p$ reaction energy levels and decay scheme.

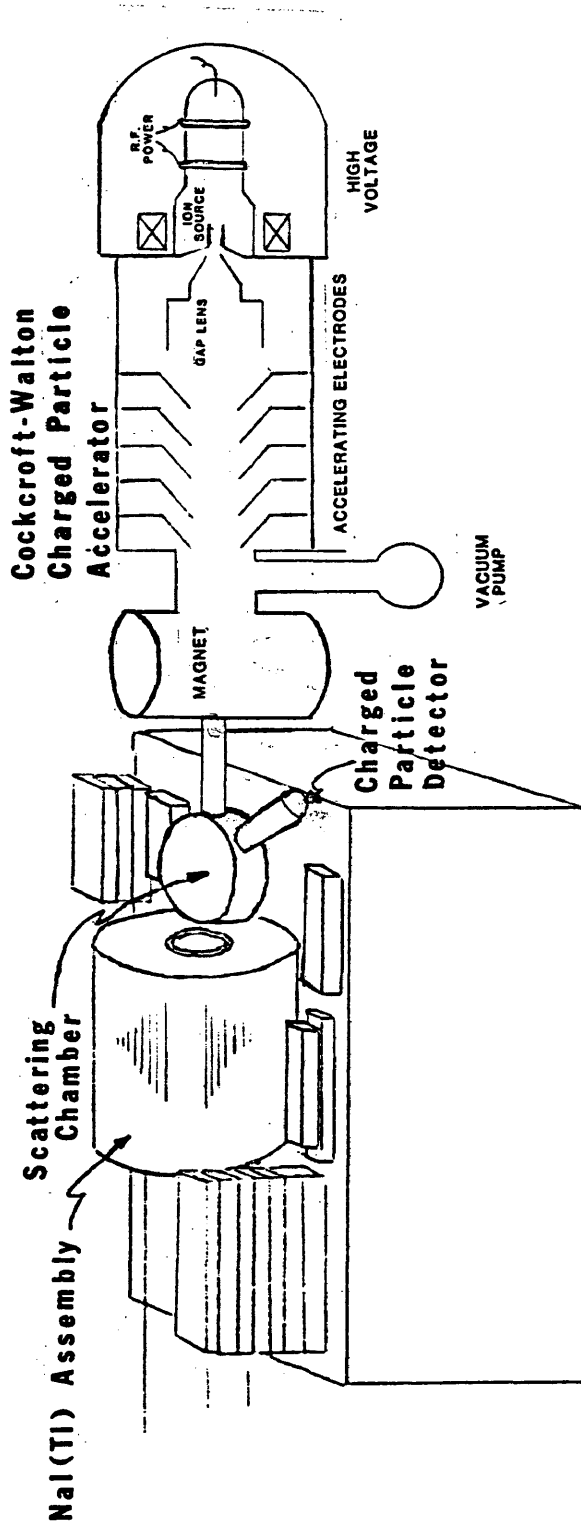


FIG. 3. Detector assembly, scattering chamber and charged particle accelerator.

was oriented at an angle of 90 degrees with respect to the magnetically analyzed beam and 33 cm. from the target so that it subtended a solid angle of 12.6 msr. This detector was protected from elastically scattered beam particles by a 2 mg/cm² aluminum foil covering. The NaI(Tl) scintillator was positioned 12.3 cm. from the target so that it subtended .54 sr. The metallic boron target was mounted on a copper block near the center of the target chamber which was 15.2 cm. in diameter.

The primary beam of the charged particle accelerator was magnetically analyzed so that unwanted charged particles contained in the beam would not reach the target, consequently the targets were located at a 45° angle from the primary beam.

Part Two. The Calculational Procedure

The described experimental arrangement made it possible, as mentioned above, to measure both the gamma ray and charged particle yields for a given reaction simultaneously. The number of gammas detected, Y_γ , is determined by the product of the detection efficiency and the thick target reaction rate for the gamma ray producing reaction. The detected gamma ray yield per incident proton with energy E_0 in the $^{11}\text{B}(p,\gamma)^{12}\text{C}$ is given by,

$$Y_{\gamma} = \epsilon_{\gamma}(E_{\gamma}) \int_{E_0}^{\infty} \frac{\Gamma_{\gamma 1}}{\Gamma_{\text{tot}}} \frac{\sigma_{\text{tot}}(E)}{\frac{dE(E)}{dn}} f(E) dE \int_{\Delta\Omega_{\gamma}} W_{\gamma}(\theta_{\gamma}) d\Omega_{\gamma} \quad (\text{II-1})$$

Similarly for the charged particle branch in the $^{11}\text{B}(p,\alpha)^8\text{Be}$ reaction, the detected number of 5.8 MeV alphas per incident proton is given by,

$$Y_{\alpha} = \epsilon_{\alpha}(E_{\alpha}) \int_{E_0}^{\infty} \frac{\Gamma_{\alpha}}{\Gamma_{\text{tot}}} \frac{\sigma_{\text{tot}}(E)}{\frac{dE(E)}{dn}} f(E) dE \int_{\Delta\Omega_{\alpha}} W_{\alpha}(\theta_{\alpha}) d\Omega_{\alpha} \quad (\text{II-2})$$

In these two equations $\epsilon(E_{\gamma})$ and $\epsilon(E_{\alpha})$ are the gamma and charged particle detector efficiencies corrected for solid angle, $\Gamma_{\gamma 1}/\Gamma_{\text{tot}}$ and $\Gamma_{\alpha}/\Gamma_{\text{tot}}$ are the gamma to total and alpha to total branching ratios respectively, $\sigma_{\text{tot}}(E)$ is the total cross section for the $^{11}\text{B} + p$ reaction, $dE(E)/dn$ is the stopping power, and $f(E)$ is the fractional density of Boron atoms in the target at an incident proton energy depth E . The final multiplicative term in each expression represents an integration of the normalized angular distribution of gamma rays and charged particles relative to the forward beam direction in the laboratory frame. The integration of these terms is done over the appropriate solid angle, that is, the solid angle subtended by either the gamma ray or charged particle

detector.

If the ratio of Eq. (II-1) and Eq. (II-2) is taken and rearranged, an expression can be obtained for the detection efficiency which is independent of the reaction cross section, the stopping powers, or the concentration of ^{11}B atoms in the target. In other words, the expression is independent of the nuclear reaction rate. The formula used to calculate the absolute detection efficiency at the energies 4.44, 11.67 and 16.11 MeV is,

$$\epsilon_{\gamma}(E_{\gamma}) = \frac{Y_{\gamma} \Gamma_{\alpha 0} \epsilon_{\alpha}(E_{\alpha}) \left\{ \int_{\Delta\Omega_{\alpha}} W_{\alpha 0}(\theta_{\alpha}) d\Omega_{\alpha} / \int_{4\pi} W_{\alpha 0}(\theta_{\alpha}) d\Omega_{\alpha} \right\}}{Y_{\alpha 0} \Gamma_{\gamma} \left\{ \int_{\Delta\Omega_{\gamma}} W_{\gamma}(\theta_{\gamma}) d\Omega_{\gamma} / \int_{4\pi} W_{\gamma}(\theta_{\gamma}) d\Omega_{\gamma} \right\}} \cdot I/I_0 \quad (\text{II-3})$$

where,

Y_{γ} - total number of gammas detected for a given energy.

$Y_{\alpha 0}$ - total number of 5.8 MeV alphas detected.

Γ_{γ} - partial width at the resonance for a particular gamma decay.

$\Gamma_{\alpha 0}$ - partial width at the resonance for alpha decay to the ^8Be ground state.

The weighting factor, $W_{\gamma}(\theta_{\gamma})$, corrects for the anisotropic production of gamma rays in the laboratory frame. These values were determined for each gamma ray in the

detector.

If the ratio of Eq. (II-1) and Eq. (II-2) is taken and rearranged, an expression can be obtained for the detection efficiency which is independent of the reaction cross section, the stopping powers, or the concentration of ^{11}B atoms in the target. In other words, the expression is independent of the nuclear reaction rate. The formula used to calculate the absolute detection efficiency at the energies 4.44, 11.67 and 16.11 MeV is,

$$\epsilon_{\gamma}(E_{\gamma}) = \frac{Y_{\gamma}\Gamma_{\alpha 0}\epsilon_{\alpha}(E_{\alpha})\{\int_{\Delta\Omega_{\alpha}}W_{\alpha 0}(\theta_{\alpha})d\Omega_{\alpha}/\int_{4\pi}W_{\alpha 0}(\theta_{\alpha})d\Omega_{\alpha}\}}{Y_{\alpha 0}\Gamma_{\gamma}\{\int_{\Delta\Omega_{\gamma}}W_{\gamma}(\theta_{\gamma})d\Omega_{\gamma}/\int_{4\pi}W_{\gamma}(\theta_{\gamma})d\Omega_{\gamma}\}} I/I_0 \quad (\text{II-3})$$

where,

Y_{γ} - total number of gammas detected for a given energy.

$Y_{\alpha 0}$ - total number of 5.8 MeV alphas detected.

Γ_{γ} - partial width at the resonance for a particular gamma decay.

$\Gamma_{\alpha 0}$ - partial width at the resonance for alpha decay to the ^8Be ground state.

The weighting factor, $W_{\gamma}(\theta_{\gamma})$, corrects for the anisotropic production of gamma rays in the laboratory frame. These values were determined for each gamma ray in the

$^{11}\text{B}(p,\gamma)^{12}\text{C}$ reaction by Grant et al. (Gr54), the results are given here:

$$W_{4.44}(\theta) \approx 1 + 0.16 \cos^2\theta, \quad (\text{II-4})$$

$$W_{11.67}(\theta) \approx 1 + 0.23 \cos^2\theta, \text{ and} \quad (\text{II-5})$$

$$W_{16.11}(\theta) \approx 1 + 0.34 \cos^2\theta. \quad (\text{II-6})$$

The other weighting factor, $W_{\alpha_0}(\theta_{\alpha_0})$, was calculated from the kinematics of the nuclear reaction (Ma68). It corrects for the anisotropic scattering of the alpha particles in the lab frame.

The term I/I_0 , includes small corrections for the attenuation of gamma rays in the target holder and the scattering chamber walls.

A negligible correction to the measured efficiency of the 16.11 MeV gamma was also made due to the summing of the 4.44 and 11.67 MeV cascade gammas.

Part Three. The Experimental Results

Spectra were recorded for the no coincidence, anti-coincidence and pair-coincidence detection modes and they are shown in Figure Four. Notice that in the anticoincidence and pair-coincidence detection modes the high energy pulses associated with cosmic rays are virtually eliminated. Also notice that the first and second escape peaks of the high energy pair produced gammas can be

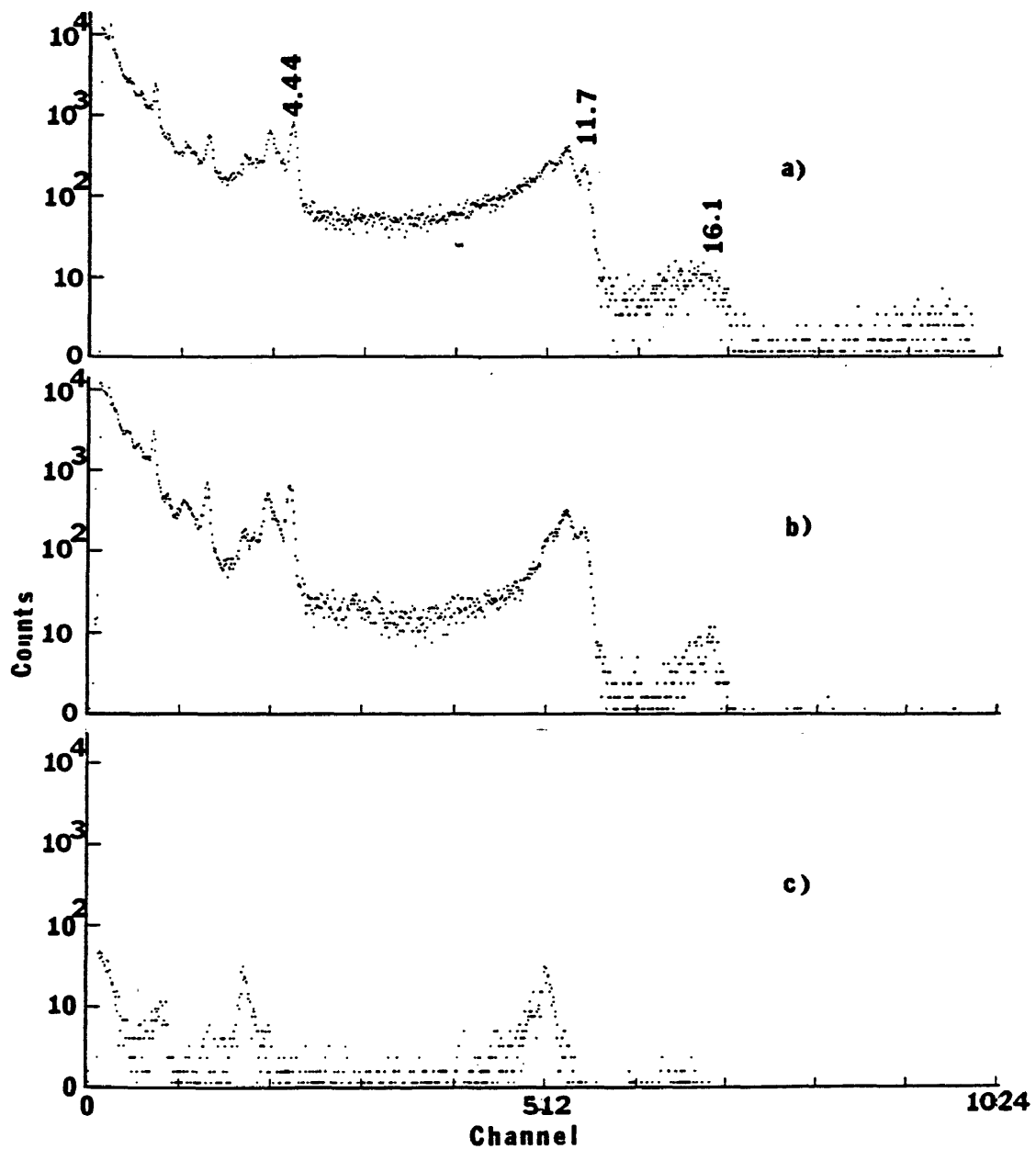


FIG. 4. The no coincidence (a), anticoincidence (b), and pair-coincidence (c) spectra for the $^{11}\text{B}(p,\gamma)^{12}\text{C}$ reaction.

resolved.

Figure Five displays a typical spectrum for the $^{11}\text{B}(p,\alpha)^8\text{Be}$ charged particle reaction. The continuum at lower energies indicates the energy which is shared by the two alpha particles as the unstable ^8Be disintegrates.

The absolute gamma ray detection efficiency for the NaI(Tl) detector was calculated for the no coincidence, anticoincidence, and pair-coincidence modes according to the procedure described in the above discussion. The experimental data along with the calculated error are given in Table Two.

The tabulated yields for the photopeak regions also include a background correction. The background was estimated by calculating the average number of counts per channel in a region immediately above the photopeak and then subtracting the appropriate number of background counts per channel from the photopeak yield. The numbers of counts in the full energy peak for the anticoincidence mode are shown in parentheses. The error in the yields were simply obtained by evaluating the statistical error in the number of counts in the photopeak region. The error values associated with the partial widths were taken from the literature (Aj68). The error for the partial width of the 16.11 MeV gamma was determined by scaling the

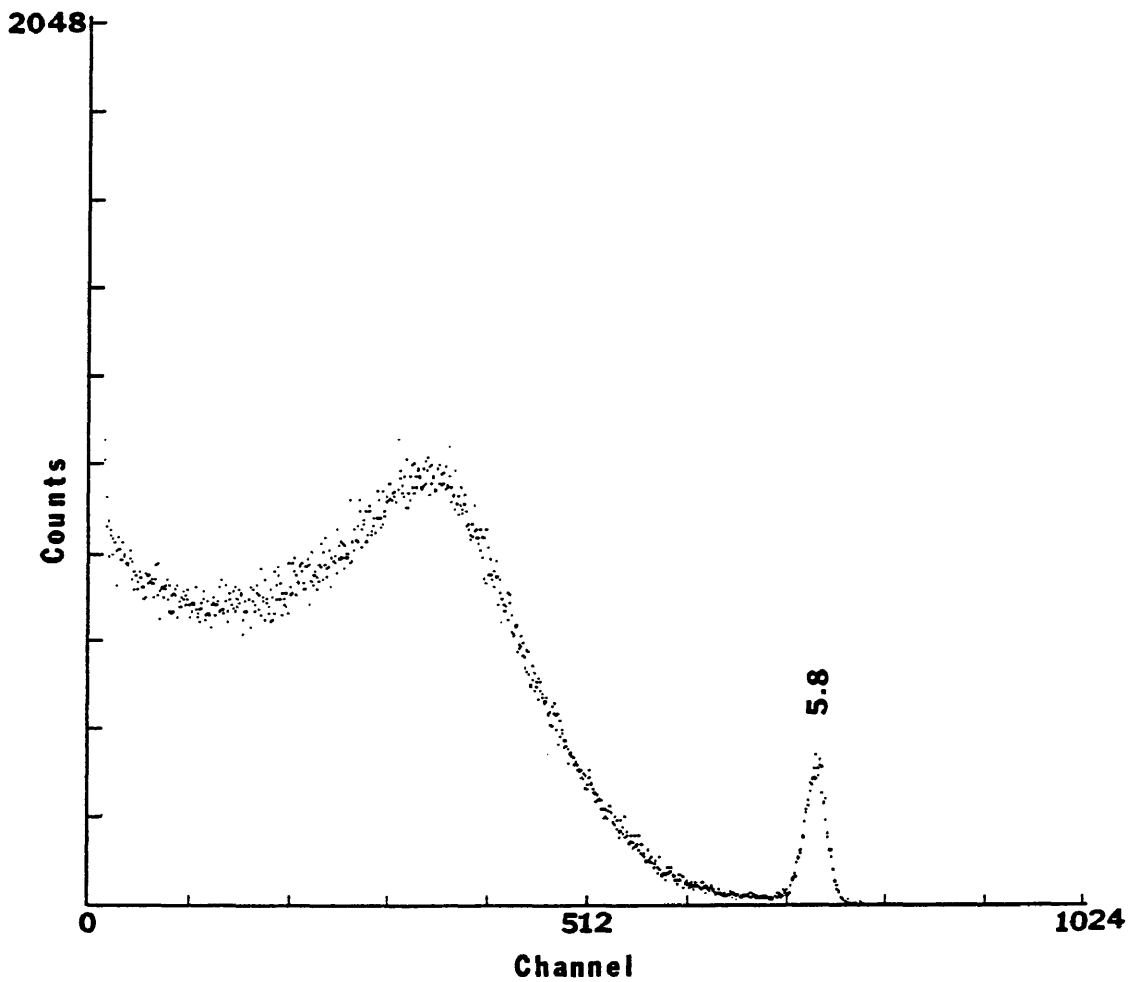


FIG. 5. Typical charged particle spectrum for the $^{11}\text{B}(p,\alpha)^8\text{Be}(2\alpha)$ reaction.

Table Two. Detection efficiency data.

<u>Experimental</u> <u>Parameter</u>	<u>Measured</u> <u>Value</u>	<u>Error</u>
<u>No coincidence</u>		
$Y_{4.44}$	20,058 cts	± 141.6 cts
$Y_{11.67}$	16,798	129.6
$Y_{16.11}$	699	26.4
$Y_{\alpha 0}$	7,600	87.2
<u>Anticoincidence</u>		
$Y_{4.44}$	15,838 (5,099)	125.8
$Y_{11.67}$	11,031 (2,005)	105.0
$Y_{16.11}$	97 (57)	19.9
$Y_{\alpha 0}$	8,335	91.3
<u>Pair-Coincidence</u>		
$Y_{4.44}$	890	29.8
$Y_{11.67}$	1,404	37.5
$Y_{16.11}$	75	8.7
$Y_{\alpha 0}$	53,321	226.5
$\Gamma_{4.44}$	21.0 eV	± 3.3 eV
$\Gamma_{11.67}$	21.0 eV	3.3 eV
$\Gamma_{16.1}$.65 eV	.27 eV
$\Gamma_{\alpha 0}$	290.0 eV	45 eV

error given in another reference (Se61).

The experimentally determined absolute detection efficiencies as a function of energy are shown graphically in Figure Six. The absolute photopeak (peak region) detection efficiencies are given for the no coincidence, anticoincidence, and pair-coincidence modes. The absolute photopeak (full energy) detection efficiency for the anticoincidence mode is also shown.

The error associated with each data point was determined by propagating the errors in the gamma yield, alpha particle yield and the reported branching ratios. The error in the 2.6 MeV data points is due only to the statistical error in counting.

A literature search revealed that the theoretical absolute detection efficiencies had been calculated up to 10.0 MeV (Ri81). R. Rieppo of the Department of Physics, University of Oulu, Linnanmaa, Finland has extended his Monte Carlo calculations up to 40 MeV in order that the theoretically expected detection efficiencies could be compared with the experimentally obtained values (Ri83). Figure Six demonstrates that the experimental and theoretical efficiencies are in good agreement.

The full energy and peak region full width half maximum (fwhm) energy resolution was calculated from the

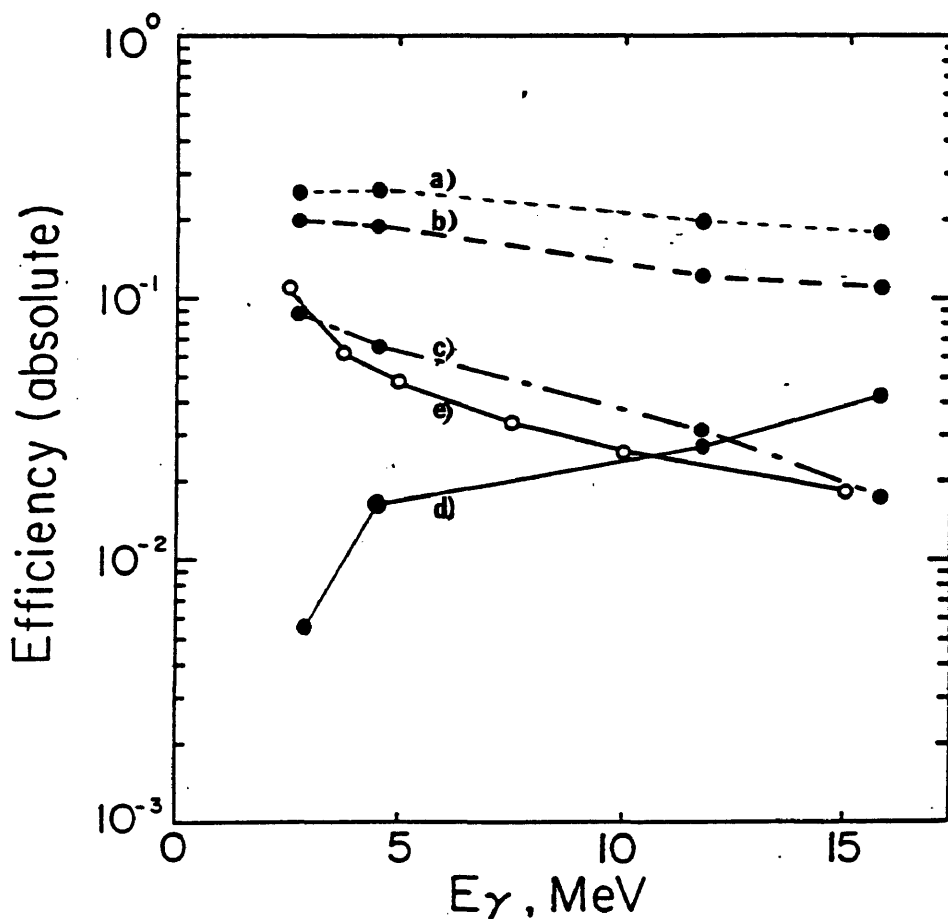


FIG. 6. The measured absolute gamma ray detection efficiencies as a function of energy for the NaI(Tl) detection system: no coincidence (peak) (a); anticoincidence, peak (b) and full energy (c); and pair-coincidence (peak) (d). The calculated absolute detection efficiency (e).

spectral data. The results are presented in Figure Seven.

The results presented in this chapter can also be found in the literature (Ce85b).

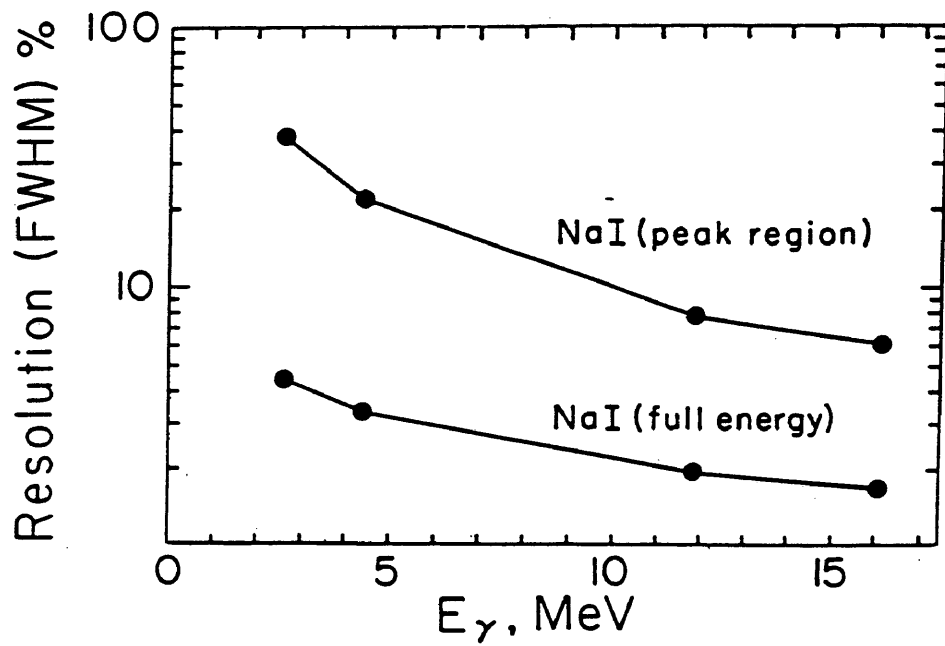


FIG. 7. Full energy and peak region fwhm energy resolution for the NaI(Tl) detector.

Chapter III. The Measurement of the $d + t$ Reaction at Low Energies

The discussion presented in this chapter focuses on the methodology used and results obtained in the measurement of the gamma ray to charged particle branching ratio for the $d + t$ reaction. The results obtained during these measurements are compared to previous measurements.

Section One. Introduction

As previously mentioned, the primary motivation for an accurate measurement of the $\Gamma_{\gamma_0}/\Gamma_{\alpha}$ branching ratio, is the potential use of the 16.76 MeV gamma as a $d + t$ fusion plasma diagnostic. For this particular application the relevant energies of interest are near the 67 keV center-of-mass resonance which corresponds to the energy at which the neutral deuterium beam will be injected into the fusion plasma in order to optimize the fusion reaction rate.

The values for the gamma ray to charged particle branching ratios which have been presented in the literature near the $d + t$ resonance are not in good agreement. The reported values range from 2×10^{-5} to 3×10^{-4} (Bu63 and Be69). This significant discrepancy established the

need for further measurements.

Two factors contribute to the extreme difficulty in measuring the $\Gamma_{\gamma_0}/\Gamma_{\alpha}$ branching ratio. Firstly, for every $d + t$ reaction only one 16.76 MeV gamma is created for every twenty thousand alpha particles emitted. Secondly, as shown schematically in Figure Eight, an alpha particle and a neutron can be emitted as the highly excited ${}^5\text{He}$ compound nucleus decays from the $3/2^+$ state. These neutrons, which can have energies of up to 14.7 MeV, can seriously interfere with any attempt to observe the 16.76 MeV gamma because of their ability to induce high energy gammas by activating the gamma detector and the surrounding materials.

Various techniques have been employed in attempting to overcome the problems associated with detecting the 16.76 MeV gamma. The earliest measurements made use of two NaI detectors, one detector was used as a gamma detector and the other was used as the alpha particle detector (Sa55). A neutron subtraction technique was then devised by interposing a Be "shadow bar" between the target and gamma detector and subsequently making measurements with and without the shadow bar. The best result that could be obtained using this technique set the branching ratio at a

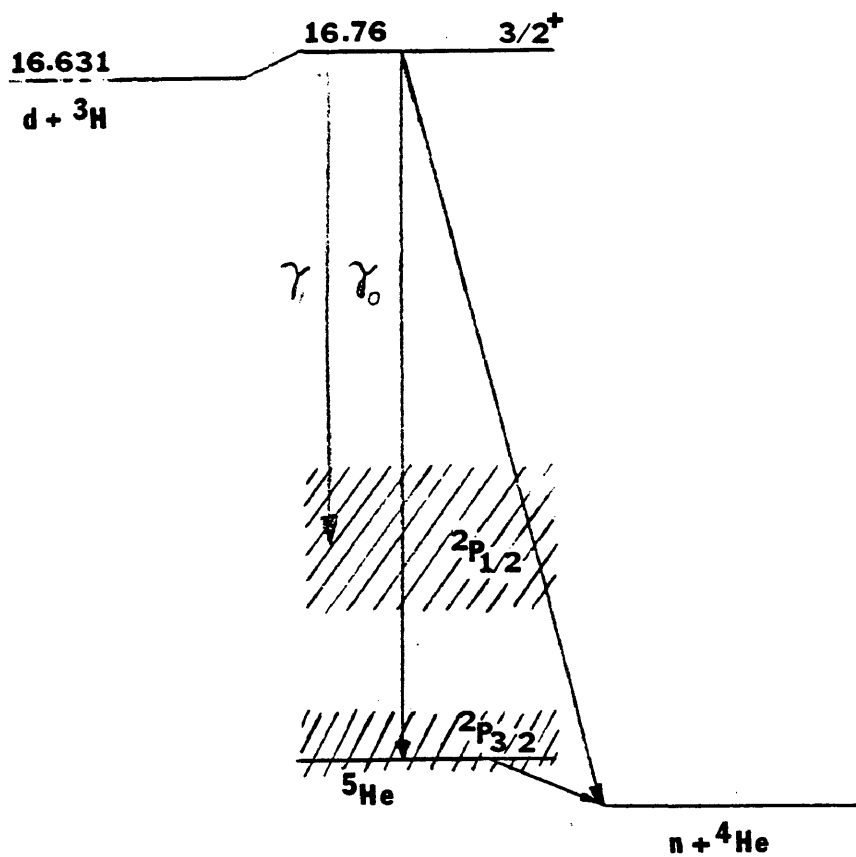


FIG. 8. The energy levels and decay scheme for the $d + t$ reaction.

value of less than 1×10^{-4} at $E_d=160\text{keV}$.

Further measurements making use of NaI gamma detectors have been done in the past but only sketchy details regarding the experimental procedure have been given (Bu63 and Be69). One paper limits its experimental discussion to the following remark (Bu63):

"... using a 5" by 5" NaI-crystal spectrometer. The crystal was placed at a distance of 1 m from the target and shielded with lead, paraffin and boron. The tritium target consisted of tritium gas absorbed in titanium metal, which had been evaporated onto a .2 mm copper backing."

Another paper (Ko70), describes using an NE 226 liquid scintillator and a time-of-flight technique to discriminate against the high neutron fluxes. At a deuteron bombarding energy of 1025 keV the branching ratio was determined to be 2.3×10^{-5} .

The significant discrepancies in the reported $\Gamma_{\gamma_0}/\Gamma_{\alpha}$ branching ratio and a limited knowledge of how the experimental data were obtained, established the need for further measurements.

Section Two. Experimental Procedure

The measurement of the $\Gamma_{\gamma_0}/\Gamma_{\alpha}$ branching ratio was determined for deuteron bombarding energies between 45 and 146 keV. The target was made of thick tritiated titanium

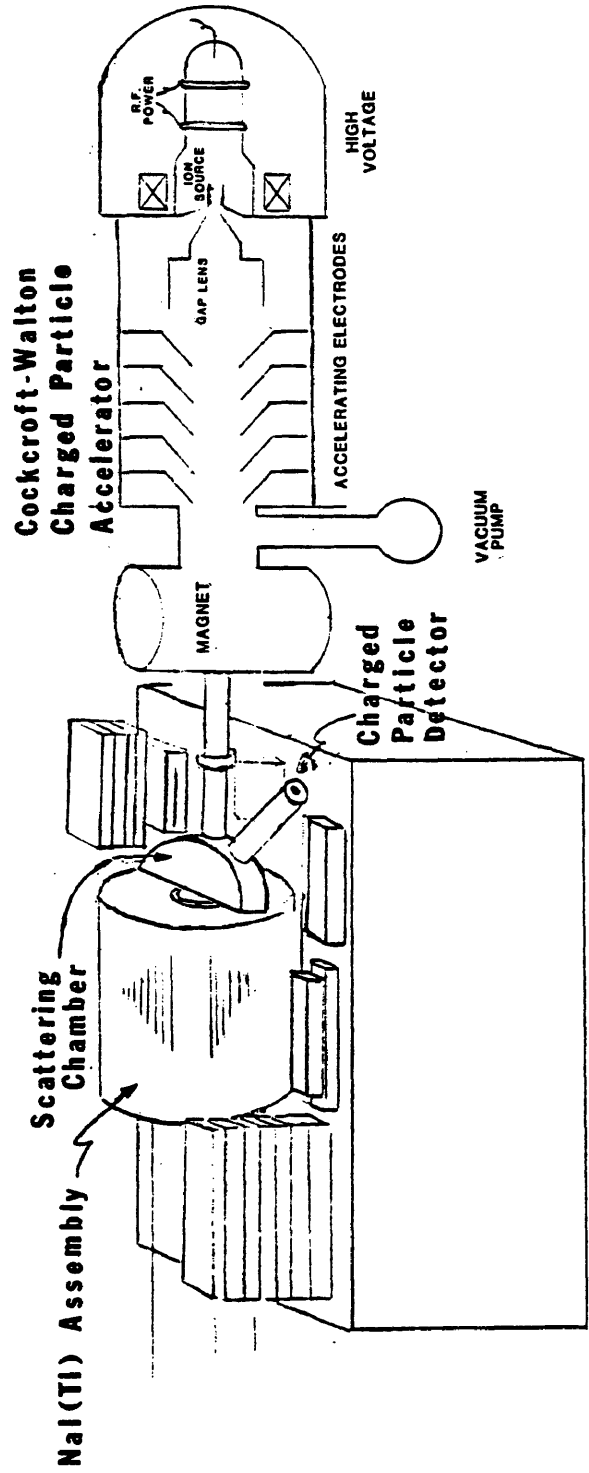


FIG. 9. The experimental layout for the $d + t$ measurements.

and it was located 3 cm. from the front face of the gamma detector. As shown in Figure Nine the scattering chamber was designed so that the gamma detector would subtend nearly 2π steradians. The plug detector used during these measurements was 3" in diameter and 3" long. The 3" x 3" plug detector was used instead of the 4" x 4" plug detector in order to eliminate some of the neutron-induced signal in the gamma spectrum. The charged particle detector subtended 12.7 msr in this arrangement.

The positioning of the gamma detector in this manner increased the probability of absorbing both the 16.76 MeV gamma of interest *and* the highly energetic neutrons associated with the ${}^4\text{He} + n$ branch of the $d + t$ reaction.

The neutron flux at the gamma detector can be calculated from the charged particle count rate. Typically this count rate was 80 cts/sec. Correcting for the solid angle of the alpha detector and the solid angle subtended by the gamma detector (nearly 2π), the resulting neutron flux at the front face of the gamma detector was 4×10^4 neutrons/sec. The corresponding gamma count rate at the face of the detector, after correcting for the efficiency of the detector, is only 25 cts/hr!

The first attempts at measuring the branching ratio $\Gamma_{\gamma_0}/\Gamma_{\alpha}$ anticipated the problem of neutron-induced gammas

in the NaI(Tl) detector. The method used in attempting to overcome this problem in the first measurements consisted of introducing various amounts of ${}^6\text{LiH}$ between the scattering chamber and the detector. The compound ${}^6\text{LiH}$ was used due to its high neutron absorption and scattering cross section. In using this technique the obvious trade-off is the reduction in the 16.76 MeV gamma count rate. Attempts to measure the branching ratio using this technique were abandoned because the gamma of interest could not be differentiated from the neutron induced gamma background.

It was determined that a significant amount of the background in the gamma spectra was due to the ${}^{127}\text{I}(n,\alpha){}^{124}\text{Sb}$ reaction in the NaI(Tl) (Bi62). As a result, a new approach was devised. The pair-coincidence spectrometry technique was successfully used in conjunction with pulse-shape discrimination to obtain sufficient 16.76 MeV gamma yields.

The pair-coincidence spectrometry technique was described in the last chapter. The pulse-shape discrimination technique (PSD) utilizes the fact that for each type of radiation that interacts with the inorganic scintillator NaI(Tl), a differently shaped light pulse is

emitted within the crystal. This technique has been previously used to study the (n,p), (n, α) and (n,n γ) reactions in NaI(Tl) (Bi62 and Ba74), but there are no references in the literature indicating that this technique has been used to study high energy gammas in the presence of intense neutron background.

The PSD in these measurements was performed by starting the time-to-amplitude converter (TAC) with the onset of the doubly differentiated pulse from the anode and stopping it with the crossover of the doubly differentiated pulse from the dynode of the plug detector. Figure Ten shows the pair-coincidence and PSD signal processing that was used in the $d + t$ measurements.

Figure Eleven shows a typical TAC spectrum. The neutron-induced alpha's are clearly separated from the gamma's. The calibration is 0.40 nsec/channel in this figure. The lower level discriminators on the start and stop channels of the TAC were set at a gamma energy of approximately 8 MeV.

Section Three. The Calculational Procedure

The total number of gammas detected can be derived from the thick target reaction rate for the gamma ray

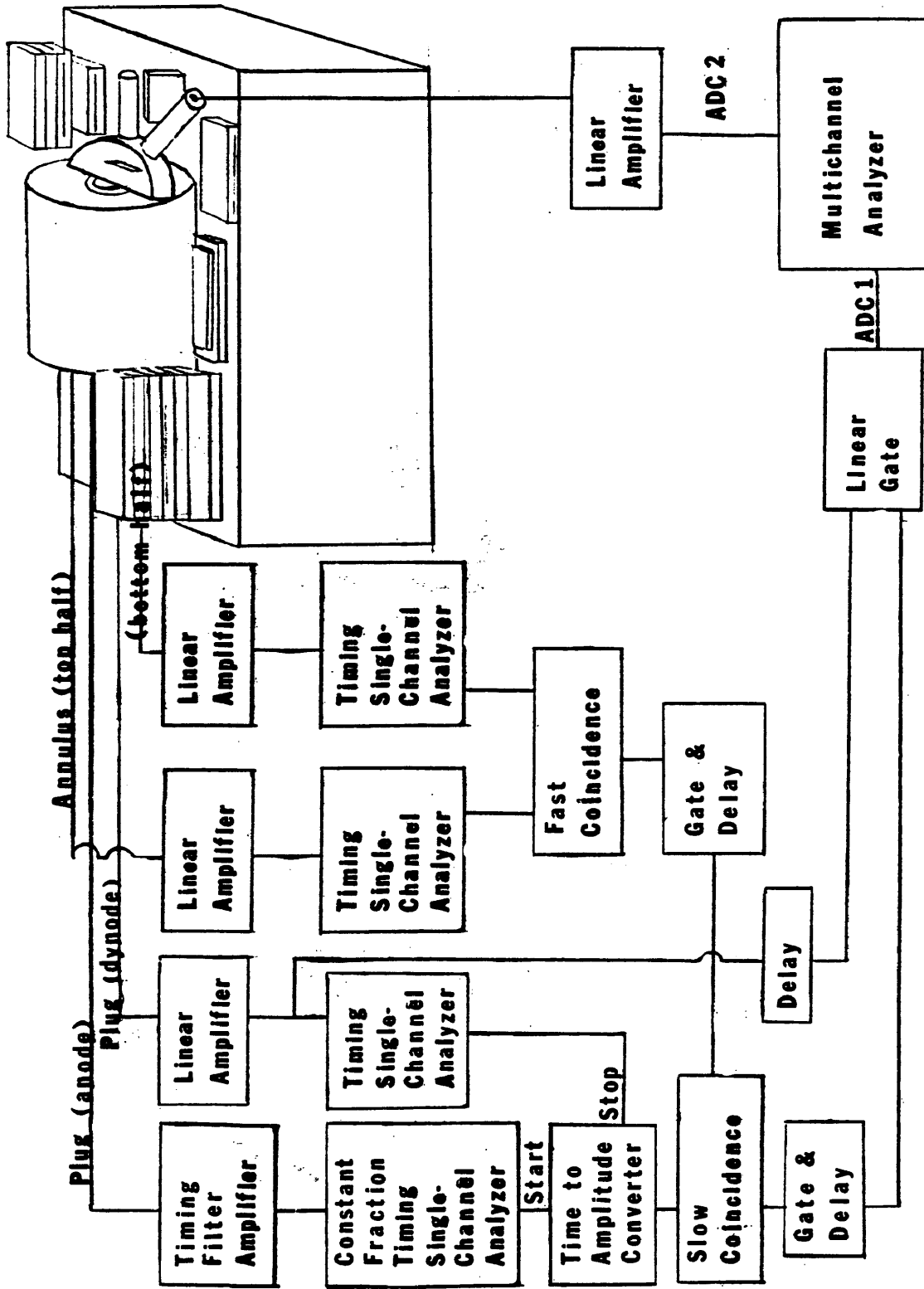


FIG. 10. Pair-coincidence and pulse-shape discrimination circuitry used for the $d + t$ measurements.

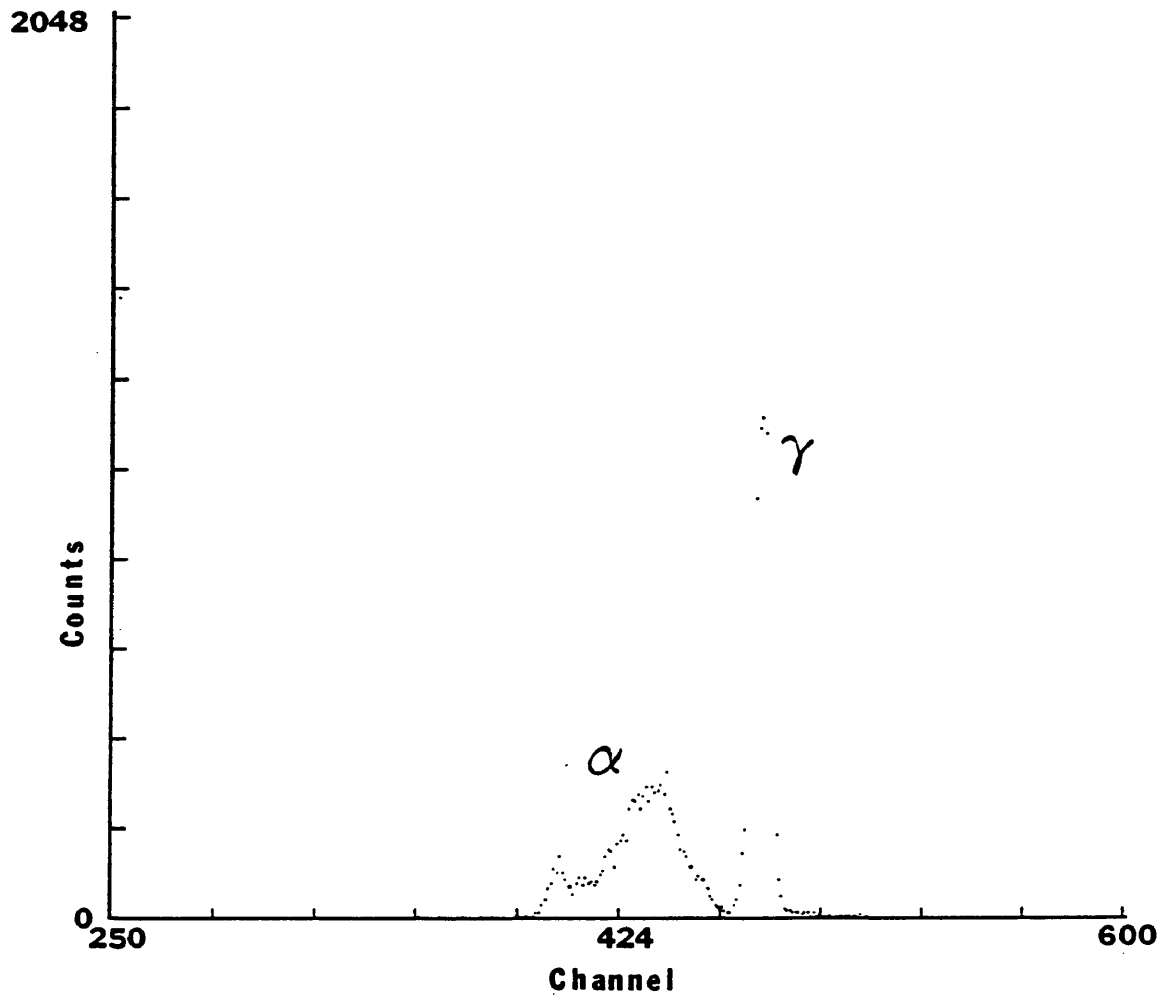


FIG. 11. Pulse-shape discrimination TAC spectrum for the $d + t$ reaction.

producing reaction. The equation that is used here, Eq. (II-1), is the same as that developed for the $^{11}\text{B}(p,\gamma)^{12}\text{C}$ reaction. The detected gamma ray yield per incident deuteron for the $^3\text{H}(d,\gamma)^5\text{He}$ reaction is given by,

$$Y_{dt\gamma} = \epsilon_{\gamma}(E_{\gamma}) \int_{E_0}^{\infty} \frac{\Gamma_{\gamma}}{\Gamma_{\text{tot}}} \frac{\sigma_{\text{tot}}(E)}{\frac{dE(E)}{dn}} f(E) dE \int_{\Delta\Omega_{\gamma}} W_{\gamma}(\theta_{\gamma}) d\Omega_{\gamma} \quad (\text{III-1})$$

Similarly for the charged particle branch in the $^3\text{H}(d,n)^4\text{He}$ reaction, the detected number of 3 MeV alphas per incident deuteron is given by,

$$Y_{dt\alpha} = \epsilon_{\alpha}(E_{\alpha}) \int_{E_0}^{\infty} \frac{\Gamma_{\alpha}}{\Gamma_{\text{tot}}} \frac{\sigma_{\text{tot}}(E)}{\frac{dE(E)}{dn}} f(E) dE \int_{\Delta\Omega_{\alpha}} W_{\alpha}(\theta_{\alpha}) d\Omega_{\alpha} \quad (\text{III-2})$$

The terms used in these expressions have been explained in Chapter II. It should be pointed out that even though the gamma detection efficiency is a function of energy, the term $\epsilon_{\gamma}(E_{\gamma})$ was taken to be nearly constant. This is reasonable since the change in efficiency is less than one percent for the maximum possible variation in energy that the incident particle could have within the target.

If the ratio of Eq. (III-1) and Eq. (III-2) is taken and it is assumed that the branching ratios $\Gamma_{\gamma 0}/\Gamma_{\text{tot}}$ and

$\Gamma_\alpha/\Gamma_{\text{tot}}$ are independent of energy, then the desired branching ratio $\Gamma_{\gamma 0}/\Gamma_\alpha$ can be written in terms of the gamma and alpha yields as follows,

$$\frac{\Gamma_{\gamma 0}}{\Gamma_\alpha} = \frac{Y_{dt\gamma}}{Y_{dt\alpha}} \frac{\epsilon_\alpha(E_\alpha)}{\epsilon_\gamma(E_\gamma)} \quad (\text{III-3})$$

The dependence on the gamma detector efficiency term can be eliminated from this expression by making use of the known branching ratios $\Gamma_{\gamma 1}/\Gamma_{\text{tot}}$ and $\Gamma_\alpha/\Gamma_{\text{tot}}$ for the $^{11}\text{B} + p$ reaction. The previous result given in Eq. (II-3) can then be rewritten as,

$$\epsilon_\gamma(E_\gamma) = \frac{Y_{Bp\gamma}}{Y_{Bp\alpha}} \frac{\Gamma_{Bp\alpha}}{\Gamma_{Bp\gamma}} \epsilon_{\alpha 0}(E_\alpha) \frac{\int_{\Delta\Omega\gamma} [W_\gamma(\theta_\gamma) A(\theta)] dt\gamma d\Omega}{\int_{\Delta\Omega\gamma} [W_\gamma(\theta_\gamma) A(\theta)]_{Bp\gamma} d\Omega} \quad (\text{III-4})$$

Here the $W_\gamma(\theta)$'s are the normalized angular distributions relative to the forward beam direction for the 11.67 MeV gamma of the $^{11}\text{B} + p$ and the 16.76 MeV gamma from the $^3\text{H} + d$ reaction in the laboratory frame. The $A(\theta)$'s are corrections for the attenuation of the gammas in the NaI(Tl) detector. Finally it should be noted that $\epsilon_{\alpha 0}(E_\alpha)$ is the efficiency for detecting 5.8 MeV $^{11}\text{B} + p$ alphas.

Using the fact that the angular distribution for the $d + t$ gammas is isotropic in the lab frame, the last term

in the numerator of Eq. (III-4) reduces to a solid angle correction.

The expression for the 11.67 MeV gamma ray angular distribution of the $^{11}\text{B}(p,\gamma)^{12}\text{C}$ reaction was given in Eq. (II-5). The 11.67 MeV gamma was used instead of the 16.11 MeV gamma since the 11.67 MeV gamma has a smaller error in its reported fractional decay width (see Table Two).

Since the charged particle detection efficiencies, $\epsilon_{\alpha_0}(E_\alpha)$ and $\epsilon_\alpha(E_\alpha)$, include the detector's solid angle, they must be corrected for the anisotropic scattering of each alpha in the lab frame. If these corrections are combined with Eq. (III-3) and Eq. (III-4) the branching ratio for the $d + t$ reaction becomes,

$$\frac{\Gamma_\gamma}{\Gamma_\alpha} = \frac{Y_{dt\gamma}}{Y_{dt\alpha}} \frac{Y_{Bp\alpha}}{Y_{Bp\gamma}} \frac{\Gamma_{Bp\gamma}}{\Gamma_{Bp\alpha}} \left[\frac{\sigma_{lab}}{\sigma_{c.m.}} \right]_{dt\alpha} \left[\frac{\sigma_{c.m.}}{\sigma_{lab}} \right]_{Bp\alpha} T \quad (\text{III-5})$$

where,

$$T = \frac{\epsilon_\gamma(E_\gamma)_{Bp\gamma}}{\epsilon_\gamma(E_\gamma)_{dt\gamma}} \left[\frac{\int_{4\pi} d\Omega}{\int_{\Delta\Omega\gamma} d\Omega} \right]_{dt\gamma} \left[\frac{\int_{\Delta\Omega\gamma} W_\gamma(\theta_\gamma) d\Omega}{\int_{4\pi} W_\gamma(\theta_\gamma) d\Omega} \right]_{Bp\gamma}$$

The above expressions have been used to calculate the branching ratio for the ground state gamma ray to charged particle for the $d + t$ reaction at low energies. This was carried out experimentally by measuring the $d + t$ and

$^{11}\text{B} + p$ reactions consecutively, while making sure that the detectors' geometry remained the same.

It should be pointed out again that this equation was derived assuming that the branching ratios $\Gamma_{\gamma_0}/\Gamma_{\text{tot}}$ and $\Gamma_{\alpha}/\Gamma_{\text{tot}}$ are independent of energy. By making this assumption the unknown branching ratio can be found without knowing any details of the reaction cross section, the number of reactions, the stopping powers, or the concentration of the tritium atoms in the target.

Section Four. Experimental Results and Discussion

Figure Twelve shows the $\text{T}(d,\gamma)^5\text{He}$ spectrum for the deuteron bombarding energy of 90 keV. As a calibration the 19.88 MeV gamma spectrum from the $\text{T}(p,\gamma)^4\text{He}$ reaction at $E_d=120$ keV, and the gamma spectrum for the $^{11}\text{B}(p,\gamma)^{12}\text{C}$ reaction is also shown along with the $d + t$ gamma spectrum. The 16.76 MeV gamma peak shown in the region of channel number 550 was also verified by introducing 1.9 cm. of lead between the target and detector. As expected, the gamma yield was reduced by 70 percent.

The branching ratios were determined for deuteron bombarding energies of 42, 52, 63, 84, 94, 125, and 146 keV. The raw data which were taken for the $d + t$

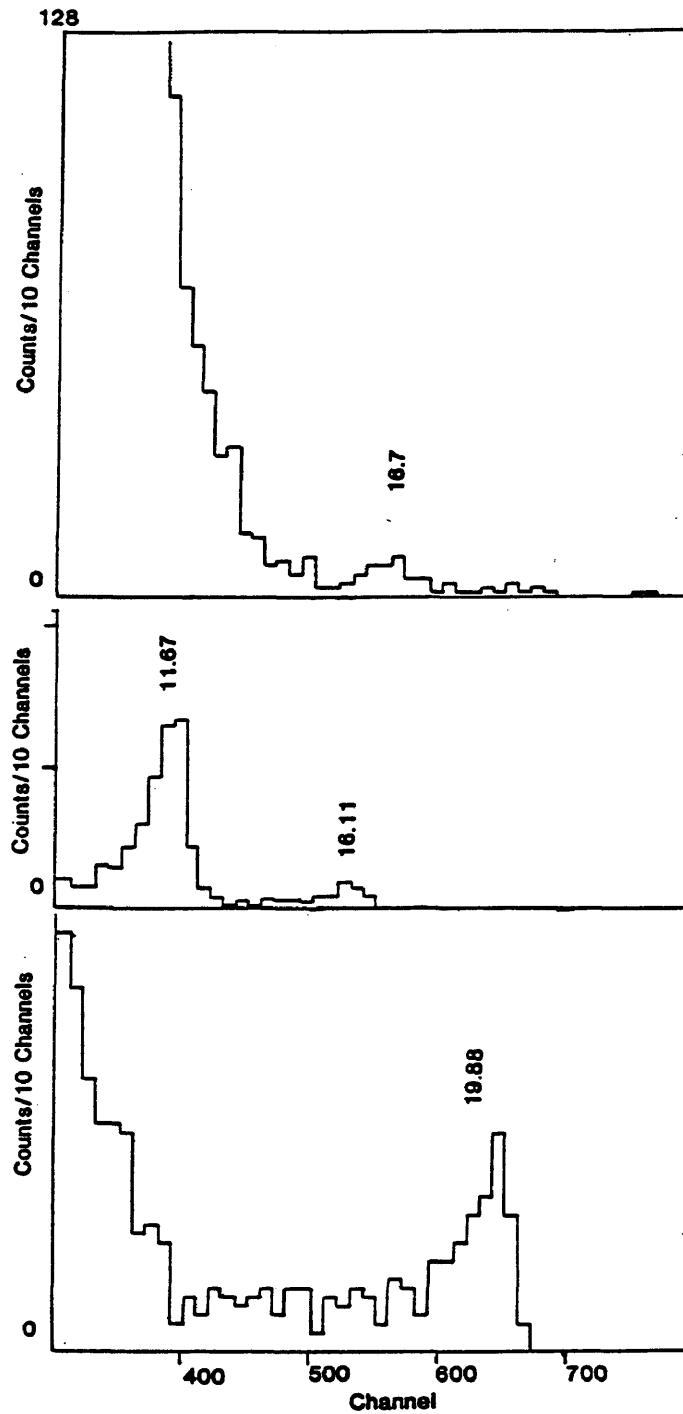


FIG. 12. $T(d,\gamma)^5\text{He}$ spectrum at $E_d=90$ keV shown along with $^{11}\text{B}(p,\gamma)^{12}\text{C}$ and $T(d,\gamma)^4\text{He}$ calibration spectra.

Table Three. $d + t$ experimental data.

E_d (keV)	Peak Gammas (cts)	Bkgd (cts)	Net (cts)	alphas (cts) ($\times 10^6$)	$\left[\frac{\sigma_{lab}}{\sigma_{c.m.}} \right] d\Omega$	$\Gamma_{\gamma_0}/\Gamma_{\alpha}$ ($\times 10^{-5}$)
44	42	16	26	1.16	.97	7.0 ± 1.9
52	99	40	59	3.26	.97	5.6 ± 1.1
63	292	94	198	7.56	.97	5.2 ± 1.7
84	186	80	106	7.17	.96	$4.5 \pm .7$
94	185	77	108	5.51	.96	$6.0 \pm .9$
125	144	56	88	5.01	.96	$5.4 \pm .9$
146	190	77	113	3.51	.95	7.2 ± 2.9

measurements are given in Table Three. The background counts for each peak were determined by subtracting the average number of background counts per channel found in the region immediately above the peak.

The other terms in Eq. (III-5) were determined as follows. After measurements it was determined that the product of the gamma to alpha branching ratio and the ratio of the alpha to gamma yields for the $^{11}\text{B} + p$ reaction reduced to a factor of 3.33.

The ratio which corrects for the anisotropic scattering of the charged particles for the $d + t$ and $^{11}\text{B} + p$ reactions in the laboratory frame was determined by

applying fundamental kinematical expressions (Ma68). The ratio for the $^{11}\text{B} + p$ reaction varies slowly over the energy range being considered here, it's value was calculated to be 1.04. The ratio for the $d + t$ reaction is tabulated above. The ratio of the detection efficiencies found in T was found to be .866 (Ri83).

The correction due to the solid angle subtended by the gamma detector for the $d + t$ gammas found in T was calculated to be 5.24. Similarly the solid angle correction for the $^{11}\text{B} + p$ gammas which includes the anisotropic distribution of gammas in the center-of-mass frame was found to be .204.

The small correction due to the difference in attenuation of the 11.67 MeV gammas and the 16.76 MeV in the target backing (copper), scattering chamber (stainless steel), and the detector housing (aluminum), resulted in only a one percent correction to the calculated branching ratio, so this correction was considered to be negligible.

The measured values of the branching ratio $\Gamma_{\gamma_0}/\Gamma_{\alpha}$ between 44 and 146 keV are shown in Figure Thirteen along with other values that have been given in the literature. The error in the branching ratios shown in Figure Thirteen corresponds to the statistical error in the gamma ray

yields of Eq. (III-5).

The measurements indicate that the branching ratio is constant over the range of 40 to 150 keV, thus confirming the initial assumption that was used in deriving the equations used to calculate the branching ratio.

The best value for these seven data points, calculated by weighted average, is

$$\Gamma_{\gamma_0}/\Gamma_{\alpha} = 5.4 \pm 1.3 \times 10^{-5}.$$

The quoted error includes a systematic error due to the uncertainty in the $\Gamma_{\gamma_1}/\Gamma_{\alpha}$ branching ratio for the $^{11}\text{B} + p$ reaction.

The results presented in this chapter have been reported in the literature (Ce84).

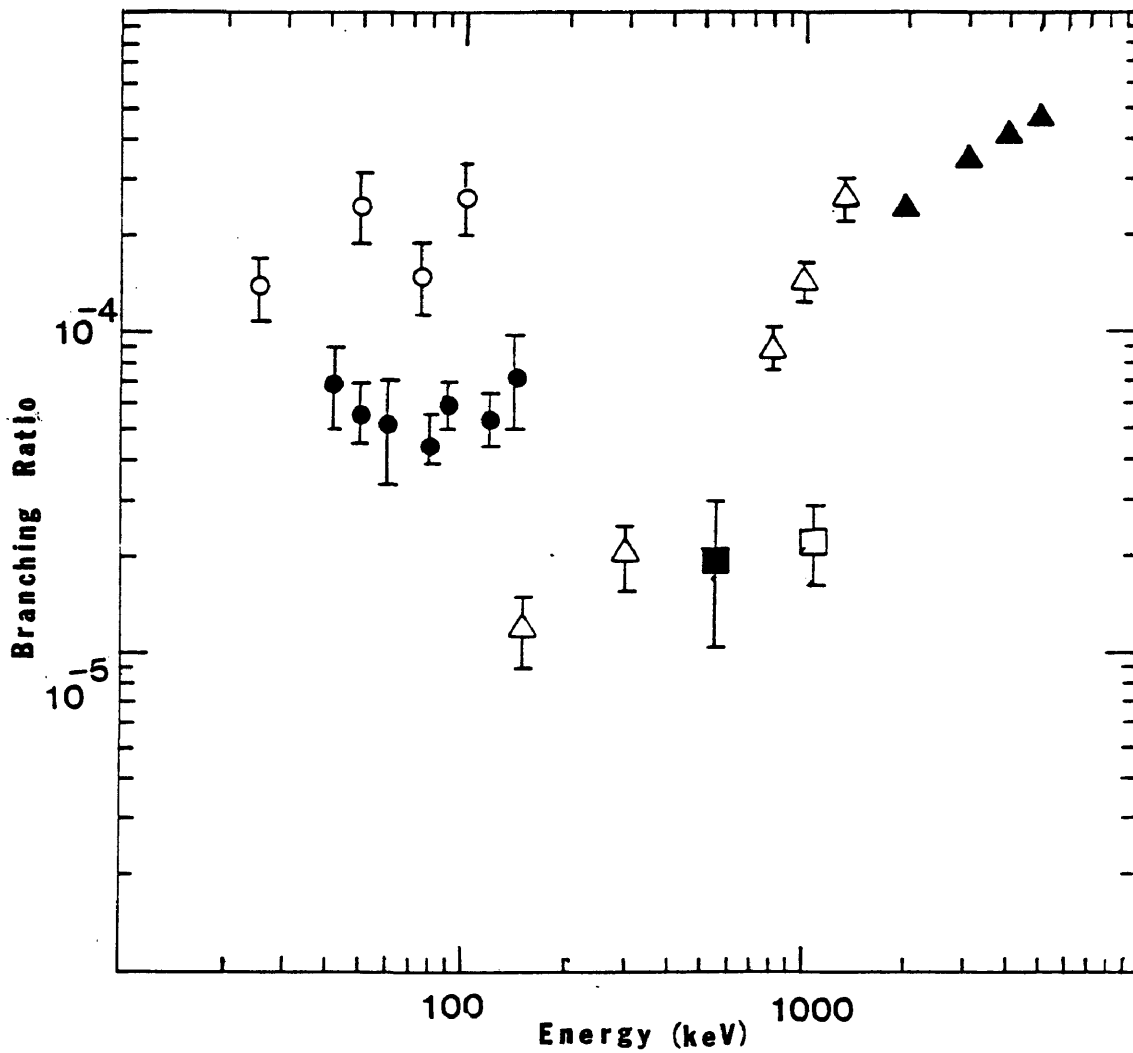


FIG. 13. Measured values of the branching ratio $\Gamma_{\gamma 0} / \Gamma_{\alpha}$ for the $d + t$ reaction. Present work, solid circles; open triangles (Bu63); solid square (Ko70); solid triangles (Ba75); open square (Co59).

ERIKHUA LARSEN LIBRARY
 COLORADO SCHOOL OF MINES
 GOLDEN, COLORADO 80401

Chapter IV. The Measurement of the $d + d$ Reaction at Low Energies.

The development of the discussion in this chapter is the same as that used in the last chapter. The experimental setup is discussed briefly and then the experimental results are presented along with some discussion.

Section One. Introduction

If the fusion plasma is treated as a Maxwellian plasma, the majority of the fusion reactions will take place in the region of the Gamow peak. For low energy distributions the Gamow peak can be determined from (Ro78)

$$E_G = [(.5)^{1/2} \pi \alpha Z_1 Z_2 \sqrt{\mu c^2 kT}]^{2/3} \quad (\text{IV-1})$$

where α is the fine structure constant, the Z 's are the nuclear charges on the reactants, μ is their reduced mass, k is the Boltzmann factor, and T is the plasma temperature in degrees Kelvin. For a deuterium plasma the value of the Gamow peak is,

$$E_G \text{ (MeV)} = .63 (kT)^{2/3} \quad (\text{IV-2})$$

where kT is in MeV. A typical deuterium plasma currently obtains temperatures in the range of 10^8 to 10^9 K. The corresponding values of the Gamow peak range from 26 keV to 123 keV. In order that the gamma from the ${}^2\text{H}(d,\gamma){}^4\text{He}$ reaction can be utilized as a fusion temperature diagnostic the branching ratio Γ_γ/Γ_p must be known in this energy region. Until the present measurements were made, this reaction had only been studied for center-of-mass energies down to 400 keV (Zu63, De69, Me69, and Po73). This fact established the need for the measurement of the branching ratio Γ_γ/Γ_p between the energies of 25 and 125 keV.

The 23.84 MeV gamma which can result from the $d + d$ reaction is indicated in the energy level diagram and associated decay scheme given in Figure Fourteen. The difficulty in measuring the unknown branching ratio at lower deuteron bombarding energies arises from the fact that only one 23.84 MeV gamma is released for every 10 million protons as the ${}^4\text{He}$ compound nucleus decays.

The methods which have been used to determine the branching ratio at higher energies have all used NaI(Tl) gamma detectors along with varying types of anticoincidence shielding to enhance cosmic-ray rejection. The experiment which measured the branching ratios for

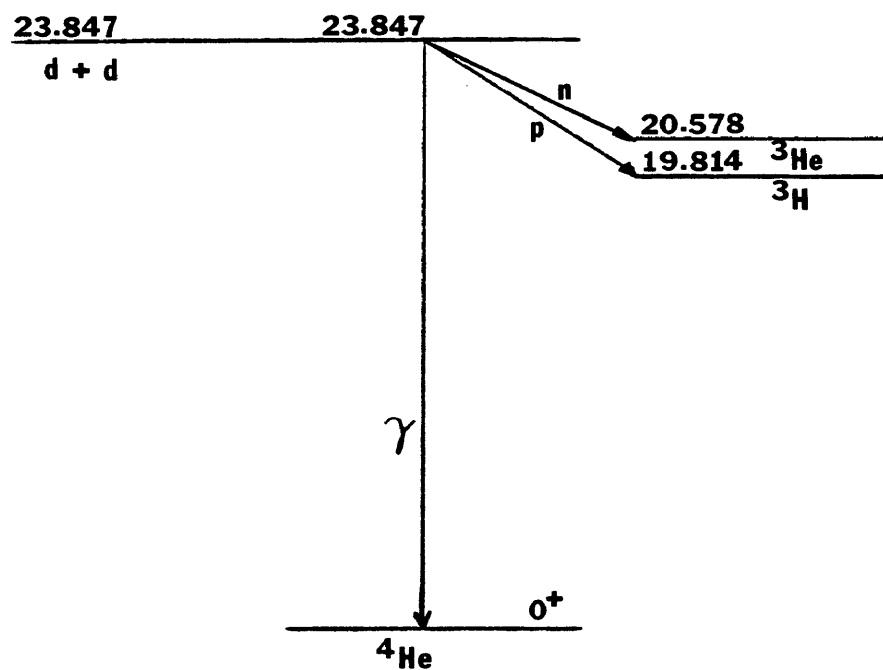


FIG. 14. The energy level diagram and decay scheme for the $d + d$ reaction.

deuteron bombarding energies near 800 keV used a 3" x 4" NaI(Tl) in conjunction with a plastic scintillator serving as an anticoincidence shield. The plastic scintillator was also surrounded with lead, to help reduce cosmic-ray background.

Section Two. Experimental Procedure

The gamma to proton branching ratio for the $d + d$ reaction was determined for deuteron bombarding energies between 52 and 157 keV. The experimental setup was very similar to that used while measuring the gamma to charged particle branching ratio for the $d + t$ reaction. The significant differences are described in the following discussion.

The same scattering chamber was used for both of the experiments; however the target was simply made by deuterating the back wall of the scattering chamber with the well-collimated deuteron beam of the charged particle accelerator. Thick target yield measurements of the ${}^2\text{H}(d,p){}^3\text{H}$ reaction verified that the target was well saturated since the deduced total cross sections were approximately in agreement with values of the total cross section found in the literature (Mi74 and Ja84). By

deuterating the wall of the scattering chamber and placing the gamma detector only a few millimeters from the target, the detector subtended nearly 2π steradians.

The 4" x 4" plug detector was used during these measurements to increase the probability of detecting the high energy gamma. The positioning of the charged particle detector allowed the simultaneous measurement of the proton yield from the ${}^2\text{H}(d,p){}^3\text{H}$ branch of the $d + d$ reaction while the gammas from the ${}^2\text{H}(d,\gamma){}^4\text{He}$ branch were being measured by the detection assembly operating in the anticoincidence mode.

Assuming a proton count rate of 1000 cts/sec at the charged particle detector, which corresponds to a typical beam current of about 15 μA , the gamma count rate for an assumed Γ_γ/Γ_p branching ratio of 1.0×10^{-7} at the NaI(Tl) detector and gamma detector efficiency of .05, was estimated to be only 18 cts/hr. The anticipated low gamma count rate indicated that run times of around three to four hours would be needed to obtain a reasonable statistical counting error.

The 4.4, 11.7, and 16.11 MeV gammas associated with the ${}^{11}\text{B} + p$ reaction and the 19.8 MeV gamma of the ${}^3\text{H}(p,\gamma){}^4\text{He}$ reaction were used once again to obtain the energy calibration and peak shape for the 23.84 MeV gamma

of the ${}^2\text{H}(d,\gamma){}^4\text{He}$ reaction.

Section Three. The Computational Procedure

The same technique that was used to find the gamma-ray to charged particle branching ratio for the $d + t$ reaction was used again in determining the Γ_γ/Γ_p branching ratio.

Again the ${}^{11}\text{B} + p$ reaction was employed so that the branching ratio could be measured independently of any knowledge of the reaction cross section, the number of reactions, the stopping powers, or the concentration of the deuterium atoms in the target. The critical assumption again is that the unknown branching ratio is assumed to be independent of energy.

The expression that was obtained and used to calculate the branching ratio for the $d + t$ reaction can be rewritten for the $d + d$ reaction as follows (cf. III-5),

$$\frac{\Gamma_\gamma}{\Gamma_p} = \frac{Y_{dd\gamma}}{Y_{ddp}} \frac{Y_{Bp\alpha}}{Y_{Bp\gamma}} \frac{\Gamma_{Bp\gamma}}{\Gamma_{Bp\alpha}} \left[\frac{\sigma_{lab}}{\sigma_{c.m.}} \right]_{ddp} \left[\frac{\sigma_{c.m.}}{\sigma_{lab}} \right]_{Bp\alpha} T \quad (\text{IV-3})$$

where,

$$T = \frac{\epsilon_\gamma(E_\gamma)_{Bp\gamma}}{\epsilon_\gamma(E_\gamma)_{dd\gamma}} \left[\frac{\int 4\pi W_\gamma(\theta) d\Omega}{\int \Delta\Omega_\gamma W_\gamma(\theta) d\Omega} \right]_{dd\gamma} \left[\frac{\int \Delta\Omega_\gamma W_\gamma(\theta_\gamma) d\Omega}{\int 4\pi W_\gamma(\theta_\gamma) d\Omega} \right]_{Bp\gamma} \left[\frac{\int \Delta\Omega_p W_p(\theta) d\Omega}{\int 4\pi W_p(\theta) d\Omega} \right]_{ddp}$$

The significant difference here is that for the $d + d$ reaction terms are included in the expression which correct for the anisotropic scattering of the protons in the center-of-mass frame and a correction for the anisotropic angular distribution of gammas (Ne84 and Po73). The angular distribution has been measured at higher energies and found to be proportional to $\sin^2\theta\cos^2\theta$ which results from the electric quadrupole multipolarity of the transition (F151).

The experimental yields were determined and the branching ratios were evaluated for center-of-mass energies of 26, 42, 52, 63, and 78 keV. The results are presented in the next section.

Section Four. Experimental Results and Discussion

The gamma-ray spectrum obtained for the ${}^2\text{H}(d,\gamma){}^4\text{He}$ reaction at $E_d=120$ keV is displayed in Figure Fifteen. The gamma of interest is clearly delineated with the centroid of the peak near channel 430.

The actual $d + d$ gamma yield for each energy was extracted from the ${}^2\text{H}(d,\gamma){}^4\text{He}$ spectrum by subtracting the cosmic-ray background and the background due to the neutron-induced reactions in the NaI(Tl). The neutron-

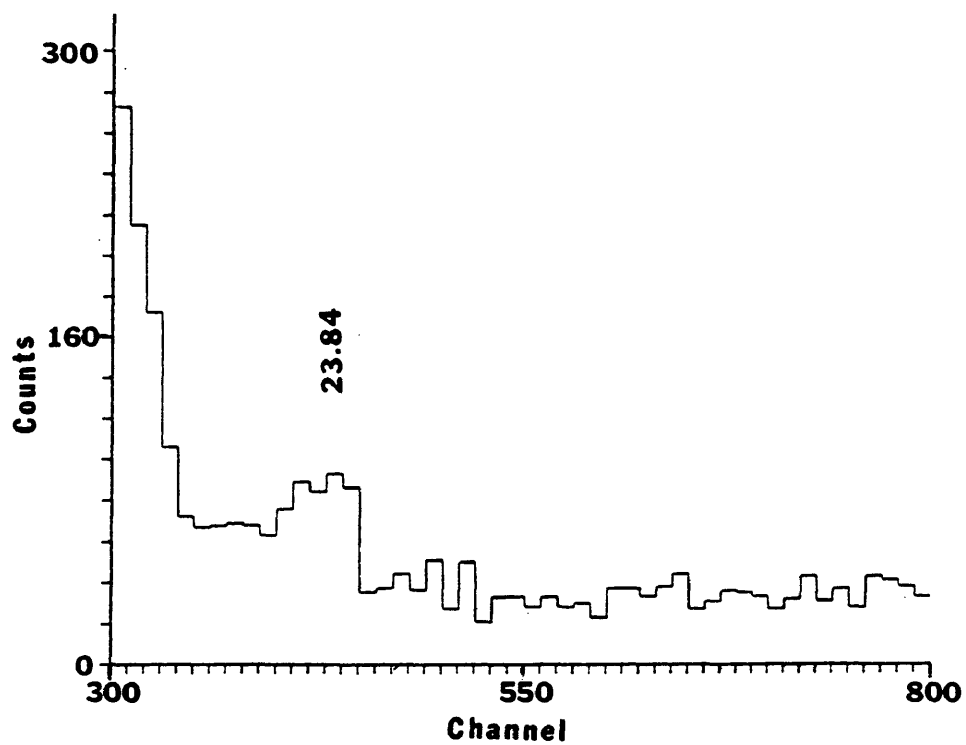


FIG. 15. The ${}^2\text{H}(d,\gamma){}^4\text{He}$ spectra for $E_d = 120$ keV.

induced background was fitted to an exponential function and any background counts that contributed to the total number of counts in the peak were subtracted out.

The experimental data that were used to calculate the branching ratios is given in Table Four. The tabulated correction due to the anisotropic scattering (A. S.) of the protons in the center-of-mass frame was taken from the literature (Ja84). The remaining terms in Eq. (IV-3) were determined as follows.

The product of the gamma to alpha branching ratio and the ratio of the alpha to gamma yields for the $^{11}\text{B} + p$ reaction was found to be .0202. The ratio which corrects for the anisotropic scattering of the protons in the laboratory frame for the $d + d$ reaction was calculated and its values are tabulated in Table Four. The same ratio for the $^{11}\text{B} + p$ reaction is 1.04. The multiplicative correction for the angular distribution of gammas in the $d + d$ reaction is given by 3.20, while the same correction for the $^{11}\text{B} + p$ gammas is .239.

The actual data points are plotted along with data points from other references in Figure Sixteen. The figure shows that the branching ratio is approximately constant over the range of bombarding energies considered here. The best value of Γ_{γ}/Γ_p for these five data points,

Table Four. $d + d$ experimental data.

E_d (keV)	Peak Gammas (cts)	Bkgd (cts)	Net (cts)	protons (cts) ($\times 10^6$)	$\left(\frac{\sigma_{lab}}{\sigma_{c.m.}} \right)_{ddp}$	A.S.	Γ_γ/Γ_p ($\times 10^{-7}$)
52	180	98	69	4.4	.809	1.05	$2.1 \pm .8$
84	543	256	287	30.3	.760	1.07	$1.3 \pm .1$
105	547	302	291	27.2	.734	1.09	$1.4 \pm .2$
125	628	397	231	29.0	.710	1.10	$.10 \pm .13$
157	344	267	151	20.6	.678	1.12	$.90 \pm .24$

calculated by weighted average, is

$$\Gamma_\gamma/\Gamma_p = 1.2 \pm 0.3 \times 10^{-7}.$$

The quoted error includes a systematic error due to the uncertainty in the $\Gamma_{\gamma 1}/\Gamma_\alpha$ branching ratio for the ${}^{11}\text{B} + p$ reaction.

The results found in this chapter are also presented in the literature (Wi85).

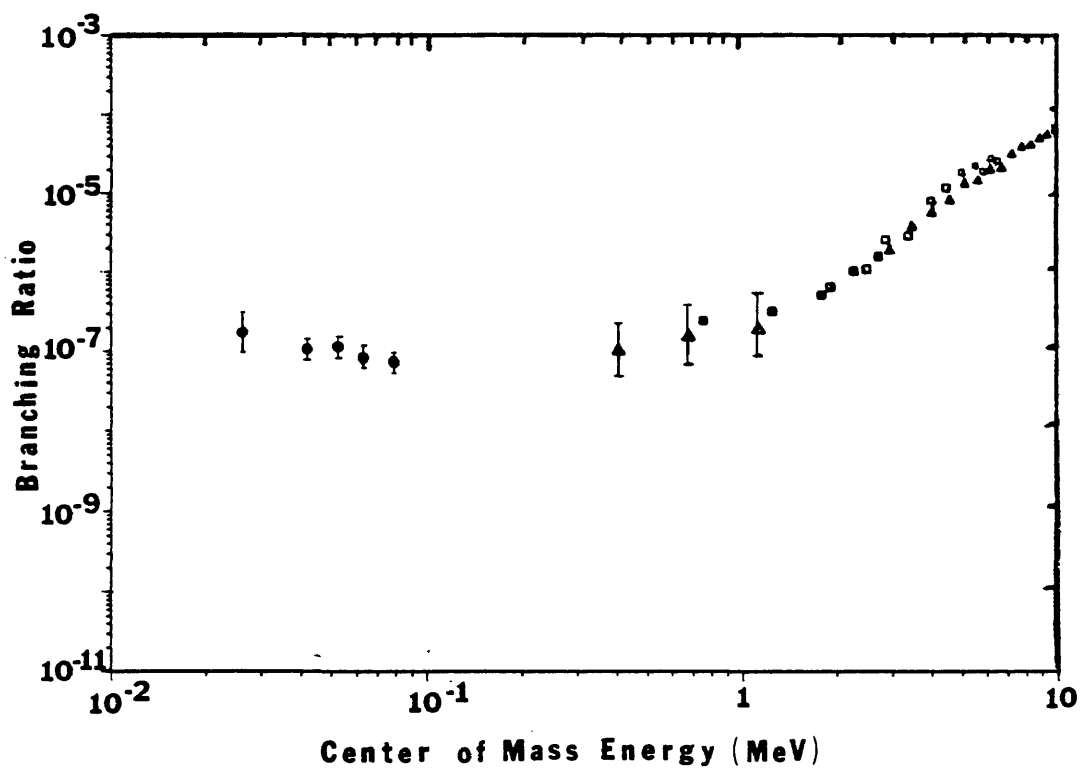


FIG. 16. Measured values of the branching ratio Γ_γ/Γ_p for the $d + d$ reaction. Present work, solid circles; open triangles, (Zu63); closed squares, (De69); open squares, (Po73); closed triangles, (Me69).

**Chapter V. The Application of the $d + t$ and $d + d$
Gammas as Fusion Plasma Diagnostics**

In this chapter the method for using the fusion gammas as a plasma temperature diagnostic will be described. The concept of reactivity which was introduced in the first chapter will be discussed in further detail here. The estimated gamma ray yields at the nuclear detector will also be presented here.

Section One. Gamma Reactivities

As pointed out in the introductory chapter the gamma ray yield can be related to the fusion plasma temperature. This is done by knowing the *gamma* reactivity for the reaction in question. The gamma reactivity can be found by using the branching ratio to scale the reactivity for the dominant charged particle branch of the reaction.

The reactivity for the charged particle branch can be found from,

$$\langle \sigma v \rangle = \int N(v) \sigma(v) v dv \quad (V-1)$$

where $N(v)$ is the Maxwellian velocity distribution, $\sigma(v)$ is the reaction cross section, and v is the relative velocity of the reactants. The Maxwellian velocity distribution of particles indicates that for increasing

temperatures less particles will occupy the states with higher energies. The functional dependence of the charged particle reaction cross section behaves in nearly an opposite manner, since the charged particle cross section increases with increasing particle energy due to the Coulomb barrier. The multiplicative product of these two functions gives a function which is generally assumed to have a Gaussian shape. The maximum of this Gaussian shaped curve is called the Gamow peak.

The cross section can be written as (C168),

$$\sigma(E) = [S(E)/E]\exp[b/E^{1/2}] \quad (V-2)$$

where,

$$b = (2\pi Z_1 Z_2 e^2 \sqrt{\mu c^2 / 2}) / hc.$$

Here $S(E)$ is known as the astrophysical S-factor and E is the interaction energy of the reactants. For nonresonant reactions the S-factor is expected to have only a weak energy dependence (Ro78). This is true for the nonresonant $d + d$ reaction.

The gamma reactivity for the ${}^2\text{H}(d,\gamma){}^4\text{He}$ reaction was determined by using Eq. (V-1) and Eq. (V-2) and then scaling by the gamma to proton branching ratio. The value of b was calculated to be $.99 \text{ MeV}^{1/2}$. The astrophysical S-factor was calculated from results given in the literature

(Ja84). The expression corrected for the center of mass frame is,

$$S(E) = (1.9 \times 10^{-2})E + 50.5 \text{ keV-barns.} \quad (V-3)$$

The calculated gamma reactivity is shown in Figure Seventeen.

The gamma reactivity for the $d + t$ reaction was found by simply scaling the known reactivity (Ri75 and Co81). These results are also given in Figure Seventeen. Notice that the DT curve has a definite peak near 67 keV due to the resonance.

Section Two. Estimated Gamma Yields

The type of calculation that is done here inherently involves several approximations. The approximations that are adopted here in calculating the gamma yield can be found in the literature (Me79). The significant approximations involve an estimate of the number density of the plasma reactants and the volume of plasma as seen by the detector. The detector efficiency, which also affects the gamma yield, can be reasonably estimated from the measurements that were reported in Chapter II.

The calculated gamma yield is for the "direct" reaction, that is, the primary fusion reaction of concern

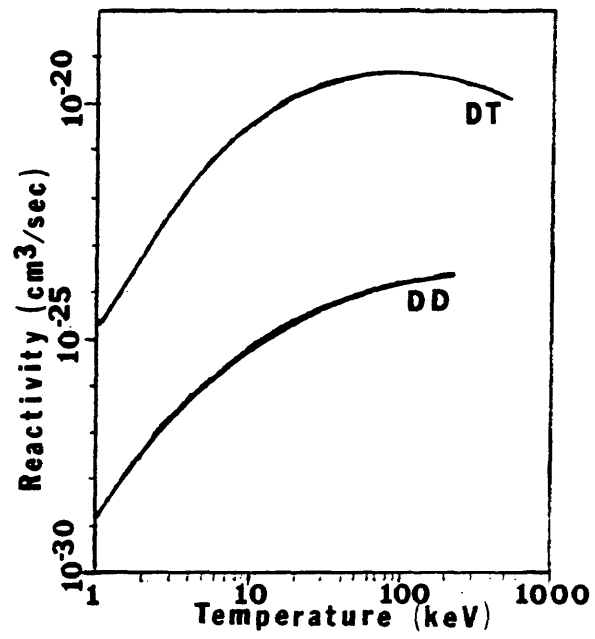


FIG. 17 The $d + t$ and $d + d$ reactivities as a function of plasma temperature.

and not secondary reactions that may occur. For example the 23.84 MeV gamma associated with the ${}^2\text{H}(d,\gamma){}^4\text{He}$ is a result of the "direct" reaction. Conceivably the 16.76 MeV gamma from the ${}^3\text{H}(d,\gamma){}^5\text{He}$ "indirect" reaction could also be detected simultaneously, since tritons are introduced into the plasma by the ${}^2\text{H}(d,p){}^3\text{H}$ reaction.

The method for finding a first estimate of the gamma yield is quite simple. The gamma count rate can be determined by correcting the reaction rate for the solid angle subtended by the detector, the efficiency of the detector, and the volume of the plasma seen by the detector. The total number of gammas produced per unit volume for a tritium target plasma with an injected deuterium beam is,

$$R = n_d n_t \langle \sigma v \rangle_\gamma. \quad (\text{V-4})$$

Here n_d and n_t are the number densities for the deuterium and tritium reactants, and $\langle \sigma v \rangle_\gamma$ is the gamma reactivity.

The gamma count rate for the same fusion plasma is then,

$$Y_\gamma = R \times \frac{d\Omega}{4\pi} \times \eta \times V \quad (\text{V-5})$$

Here the corrections for the solid angle subtended by the detector, the efficiency of the detector, and the volume of plasma being observed are taken into account. For these calculations the distance from the plasma to

detector R, is estimated to be 400 cm. The radius of the cylindrical NaI(Tl) detector is set at 5.1 cm.

The efficiency of the detector for 16.76 Mev gammas can be taken from Figure Six (pg. 23). The value is about .13. The efficiency for the 23.84 MeV gammas is about .10. The anticipated placement of the detector outside the Tokamak Fusion Test Reactor (TFTR) is shown in Figure Eighteen. With this type of arrangement the plasma volume is collimated so that the effective volume as seen by the detector is a cylinder with radius of 10 cm and length of about 50 cm. This corresponds to a plasma volume of $1.7 \times 10^4 \text{ cm}^3$.

It should be pointed out that any attenuation due to the geometry of the port which the gammas pass through before they reach the detector has been ignored.

For a first estimate it is reasonable to assume that both reactive constituents have number densities equal to about $7 \times 10^{13} \text{ cm}^{-3}$. The resulting gamma count rates for the $d + t$ and $d + d$ reactions are given in Figure Nineteen. On the basis of the calculations made here it seems reasonable that the measurement of fusion gammas should provide an independent temperature diagnostic for the $d + t$ and $d + d$ fusion reactors.

It should be noted that the neutral injection beams

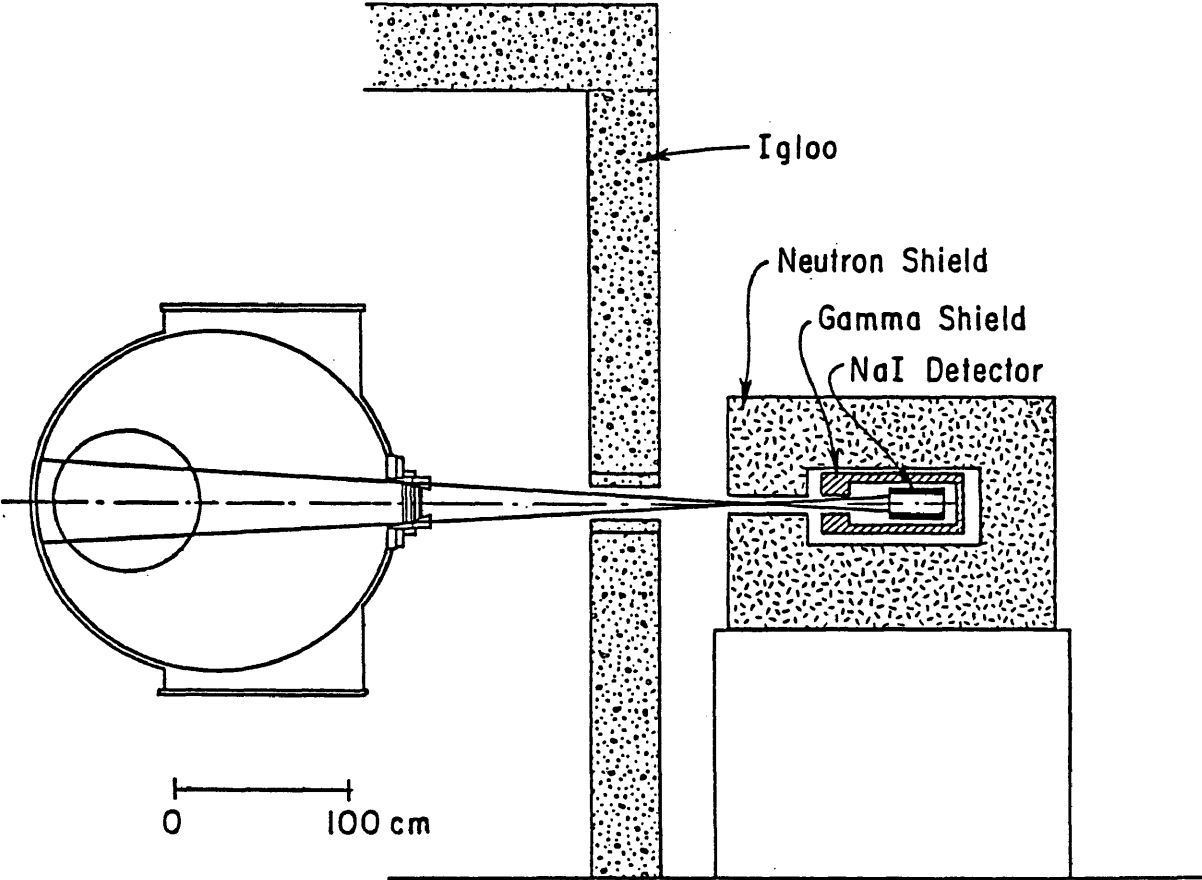


FIG. 18. Detector placement outside the TFTR (Me79).

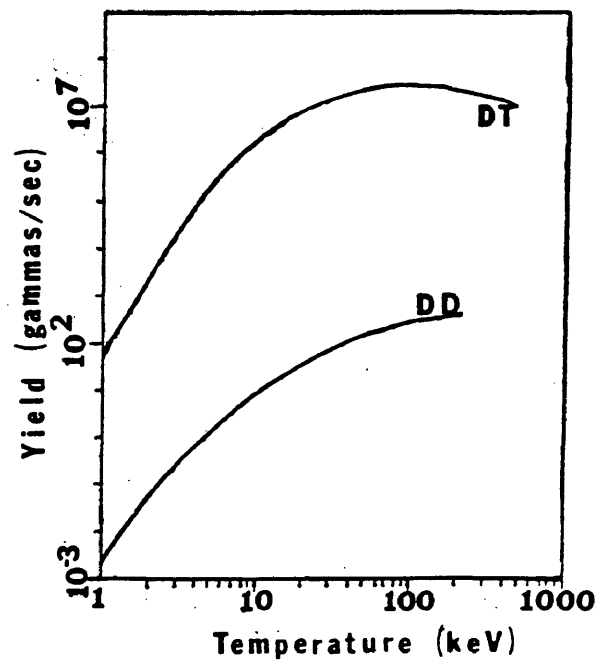


FIG. 19. Estimated gamma yields for the $d + t$ and $d + d$ fusion plasmas.

are pulsed for durations of 100 to 200 ms. Even with the gamma production limited to this time interval the use of fusion gammas as a temperature diagnostic should be justified for a DT plasma for temperatures as low as 3 or 4 keV, which are well below the 67 keV center-of-mass resonance.

In the case of a DD plasma the gamma count rate corresponding to a temperature of 200 keV would only be about 275 gammas/sec. To improve this count rate the solid angle subtended by the detector would have to be increased to compensate for the lower gamma reactivity. Increasing the plasma volume by enlarging the port would also improve the gamma count rate.

References Cited

- (Aj68) F. Ajzenberg-Selove and T. Lauritson, *Nucl. Phys.*, **A114**, (1968).
- (Ba74) C.M. Bartle, *Nucl. Instr. Methods* **124**, 547 (1974).
- (Bi62) P.G. Bizetti, A.M. Bizetti-Sona, and M. Bocciolini, *Nucl. Phys.* **36**, 38 (1962).
- (Be69) V.M. Bezotosnyi et al., *Yad. Fiz.* **10**, 225 (1963).
- (Bu63) W. Buss, H. Waffler, and B. Ziegler, *Phys. Lett.* **4**, 198 (1963).
- (Ce84) F.E. Cecil and F.J. Wilkinson III, *Phys. Rev. Lett.* **53**, 767 (1984).
- (Ce85) F.E. Cecil, D.M. Cole, R. Philbin, N. Jarmie, and R.E. Brown, *Phys. Rev. C.*, **32**, 690 (1985).
- (Ce85b) F.E. Cecil, F.J. Wilkinson III, R.A. Ristinen, and R. Rieppo, *Nucl. Instr. Methods* **A234**, 479 (1985).
- (Cl68) D.D. Clayton, **Principles of Stellar Evolution and Nucleosynthesis**, (McGraw-Hill, 1968).
- (Co85) D.M. Cole, M. S. thesis, Colorado School of Mines, 1985 (unpublished).
- (Co81) R.W. Conn, in **Fusion**, Ed. by E. Teller, 1 Part B, 199 (Academic Press, 1981).
- (Co59) J. Coon and R. Davis, *Bull. Am. Phys. Soc.* **4**, 365

- (1959).
- (De69) A. Degre, M.Schaeffer, and M. Suffert, private communication to Meyerhof, see (Me69).
- (Gr54) P.J. Grant, F.C. Flack, J.G. Rutherglen, and W.M. Deuchars, Proc. Phys. Soc. London, Sect A **67**, 751 (1954).
- (Ja84) N. Jarmie, R.E. Brown, and R.A. Hardekopf, Phys. Rev. C **29**, 2031 (1984); N. Jarmie and R.E. Brown, Los Alamos National Laboratory Report LA-UR-84-3349, 1984.
- (Ko70) A. Kosiare and H.B. Willard, Phys. Lett. **32B**, 99 (1970).
- (Ma78) G. Magyar, Nuclear Fusion, **18**, (1978).
- (Ma68) J.B. Marion and F.C. Young, **Nuclear Reaction Analysis**, (North-Holland, Amsterdam, 1968).
- (Me79) S.S. Medley and H.D. Campbell, Princeton Plasma Physics Laboratory Report, TFTR-TM-11, 1979.
- (Me82) S.S. Medley and H. Hendel, Bull. Am. Phys. Soc., **26**, 980 (1982), and Princeton Plasma Physics Laboratory Report No. PPPL-1950, 1982 (unpublished).
- (Me67) W.E. Meyerhoff, **Elements of Nuclear Physics**, (McGraw-Hill, 1967).
- (Me69) W.E. Meyerhof, W. Feldman, S. Gilbert, and W.

- O'Connel, Nucl. Phys. **A131**, 489 (1969).
- (Mi74) G.H. Miley, H. Towner, and N. Ivich, University of Illinois Report No. C00-2218-17, 1974.
- (Ne84) D.E. Newman and F.E. Cecil, Nucl. Instr. Methods **227**, 339 (1984).
- (Po73) J.M. Poutissou and W. Del Bianco, Nucl. Phys. **A199**, 517 (1973).
- (Ri75) F.L. Ribe, Rev. Mod. Phys. **47**, 1 (1975).
- (Ri81) R. Rieppo, Int. J. Appl. Radiat. Isot. **32**, 254 (1981).
- (Ri83) R. Rieppo, private communication, (1983).
- (Ro78) C. Rolfs and H.P. Trautvetter, Annu. Rev. Nucl. Part. Sci. **28**, 122 (1978).
- (Sa55) G.A. Sawyer and L.C. Burkhardt, Phys. Rev. **98**, 1305 (1955).
- (Sc85) J.C. Scorby, M. S. thesis, Colorado School of Mines, 1985 (unpublished).
- (Se61) R.E. Segal and M.J. Bina, Phys. Rev. **124**, 814 (1961).
- (Wh79) C.B. Wharton, **Physics Today**, **5**, (1979).
- (Wi85) F.J. Wilkinson III and F.E. Cecil, Phys. Rev. C, **31**, 2036 (1985).
- (Zu63) R.W. Zurmuhle, W.E. Stephens, and H.H. Staub, Phys. Rev. **132**, 751 (1963).

Appendix. Reaction Yields

The purpose of this appendix is to elucidate the origin of the gamma ray yield equations that are used in the text. The yield equations, such as Eq. (II-1), give the total number of gammas detected per incident beam particle. Derivations of the yield equation, similar to the one presented here, can be found in basic nuclear physics texts (Me67).

The starting point for this derivation is the definition of the nuclear cross section. Recall that the cross section for the light product in a nuclear reaction is stated as: the number of light product particles per unit time, per unit incident flux, and per target nucleus. The expression for the cross section can be written as,

$$\sigma = \frac{N}{(I/A)(n)(A)(\Delta x)}. \quad (\text{App-1})$$

Here N is the number of light particles produced per unit time, I/A is the number of incident particles per unit time per unit area, n is the number of target nuclei per unit volume, A is the area over which the incident beam is striking, and Δx is the target thickness. Note that this expression gives the *light particle cross section*. The

light particle cross section, for example a gamma ray, is related to the total cross section by the branching ratio as follows,

$$\sigma_{\gamma}(E) = \sigma_{\text{tot}}(E) \frac{\Gamma_{\gamma}}{\Gamma_{\text{tot}}}. \quad (\text{App-2})$$

It is also important to note that the cross section can be a function of energy as indicated in Eq. (App-2).

An expression for the gamma ray yield per incident particle, Y_{γ} , can be obtained by rearranging Eq. (App-1),

$$Y_{\gamma} = N/I = (\sigma_{\gamma})(n)(\Delta x). \quad (\text{App-3})$$

For thick target calculations the expression on the right hand side is integrated over the range which the incident particles penetrate into the target. The resulting expression is simply,

$$Y_{\gamma} = \int_0^R \sigma_{\gamma} n \, dx. \quad (\text{App-4})$$

This expression can be written in terms of energy by using the fact that the differential change in energy per differential change in depth is given by,

$$dE/dx = n (dE/dn'). \quad (\text{App-5})$$

Here n' signifies and areal number density of target atoms.

Equation (II-1) can be reproduced by combining Eqs. (App-2), (App-4), and (App-5) along with the following corrections: the detection efficiency of the nuclear detector, the fractional density of target atoms in the target at a depth corresponding to an energy E , and the solid angle subtended by the nuclear detector. Note too that the prime has been dropped from the variable signifying the areal number density of particles. The result is,

$$Y_{\gamma} = \epsilon_{\gamma}(E_{\gamma}) \int_{E_0}^{\infty} \frac{\Gamma_{\gamma}}{\Gamma_{\text{tot}}} \frac{\sigma_{\text{tot}}(E)}{\frac{dE(E)}{dn}} f(E) dE \int_{\Delta\Omega_{\gamma}} W_{\gamma}(\theta_{\gamma}) d\Omega_{\gamma} \quad (\text{II-1})$$